Trends in atmospheric evaporative demand in Great Britain using high-resolution meteorological data

Emma L. Robinson[1], Eleanor M. Blyth[1], Douglas B. Clark[1], Jon Finch[1] and Alison C. Rudd[1]

[1]{Centre for Ecology and Hydrology, Maclean Building, Benson Lane, Crowmarsh Gifford, Wallingford OX10 8BB}

Correspondence to: Emma L. Robinson (emrobi@ceh.ac.uk)

10   **Abstract**

11   Observations of climate are often available on very different spatial scales from observations

12   of the natural environments and resources that are affected by climate change. In order to help

13   bridge the gap between these scales using modelling, a new dataset of daily meteorological

14   variables was created at 1 km resolution over Great Britain for the years 1961-2012, by

15   interpolating coarser resolution climate data and including the effect of local topography. These

16   variables were used to calculate atmospheric evaporative demand (AED) at the same spatial

17   and temporal resolution. Two functions that represent AED were chosen: one is a standard form

18   of Potential Evapotranspiration (PET) and the other is a derivative of it used by hydrologists

19   that includes the effect of water intercepted by the canopy (PETI). Temporal trends in these

20   functions were calculated, with PET found to be increasing in all regions, and at an overall rate

21   of 0.021 ± 0.021 mm d^{-1} decade^{-1} in Great Britain, while PETI was found to be increasing at a

22   rate 0.023 ± 0.023 mm d^{-1} decade^{-1} in England (0.028 ± 0.025 mm d^{-1} decade^{-1} in the English

23   Lowlands), but not increasing at a statistically significant rate in Scotland or Wales. The trends

24   were found to vary by season, with spring PET increasing by 0.043 ± 0.019 mm d^{-1} decade^{-1}

25   (0.038 ± 0.018 mm d^{-1} decade^{-1} when the interception correction is included) in Great Britain,

26   while there is no statistically significant trend in other seasons. The trends were attributed

27   analytically to trends in the climate variables; the overall positive trend was predominantly

28   driven by rising air temperature, although rising specific humidity had a negative effect on the

29   trend. Increasing downward short- and longwave radiation made an overall positive

30   contribution to the PET trend, while the 10 m wind speed had a negative effect. The trend in

31   spring PET was particularly strong due to a strong increase in spring downward shortwave

32   radiation.

1 Introduction

There are many studies showing the ways in which our living environment is changing over time: changing global temperatures (IPCC, 2013), radiation (Wild, 2009) and wind speeds (McVicar et al., 2012) can have significant impacts on ecosystems and human life (IPCC, 2014a). While there are overall global trends, the impacts can vary between regions (IPCC, 2014b). In the UK, wildlife surveys of both flora (Wood et al., 2015; Evans et al., 2008) and fauna (Pocock et al., 2015) show a shift in patterns and timing (Thackeray et al., 2010). In addition, the UK natural resources of freshwater (Watts et al., 2015), soils (Reynolds et al., 2013; Bellamy et al., 2005) and vegetation (Berry et al., 2002; Hickling et al., 2006; Norton et al., 2012) are changing. The UK is experiencing new environmental stresses on the land and water systems through changes in temperature and river flows (Crooks and Kay, 2015; Watts et al., 2015; Hannaford, 2015), which is part of a widespread global pattern of temperature increase and circulation changes (Watts et al., 2015).

To explain these changes in terms of climate drivers, there are several gridded meteorological datasets available at global and regional scales. Global datasets can be based on observations – for example the 0.5° resolution Climate Research Unit time series 3.21 (CRU TS 3.21) data (Jones and Harris, 2013; Harris et al., 2014) – while some are based on global meteorological reanalyses bias-corrected to observations – for example the WATCH Forcing Data (WFD, 0.5°; Weedon et al. (2011)), the WATCH Forcing Data methodology applied to ERA-Interim reanalysis product (WFDEI, 0.5°; Weedon et al. (2014)) and the Princeton Global Meteorological Forcing Dataset (1°; Sheffield et al. (2006)). At the regional scale in Great Britain (GB), there are datasets that are derived directly from observations – for example the Met Office Rainfall and Evaporation Calculation System (MORECS) dataset at 40 km resolution (Thompson et al., 1981; Hough and Jones, 1997) and the UKCP09 observed climate data at 5 km resolution (Jenkins et al., 2008).

However, while regional observations of carbon, methane and water emissions from the land (Baldocchi et al., 1996), the vegetation cover (Morton et al., 2011) and soil properties (FAO/IIASA/ISRIC/ISS-CAS/JRC, 2012) are typically made at the finer landscape scale of 100 m to 1000 m, most of these long-term gridded meteorological datasets are only available at a relatively coarse resolution of a few tens of km. These spatial scales may not be representative of the climate experienced by the flora and fauna being studied, and it has also been shown that input resolution can have a strong effect on the performance of hydrological

models (Kay et al., 2015). In addition, the coarse temporal resolution of some datasets, for example the monthly CRU TS 3.21 data (Harris et al., 2014; Jones and Harris, 2013), can miss important sub-monthly extremes.

Regional studies are important to identify drivers and impacts of changing meteorology that may or may not be reflected in trends in global means. For example, in Canada (Vincent et al., 2015) and Europe (Fleig et al., 2015), high resolution meteorological data have been used to identify the impacts of changing circulation patterns, while in Australia wind speed data have been used to quantify the effects of global stilling in the region (McVicar et al., 2008). While there are datasets available at finer spatial and temporal resolutions for the UK (such as UKCP09 (Jenkins et al., 2008)), these often do not provide all the variables needed to identify the impacts of changing climate.

To address this, we have created a meteorological dataset for Great Britain at 1 km resolution (Robinson et al., 2015a). It is derived from the observation-based MORECS dataset (Thompson et al., 1981; Hough and Jones, 1997), and then downscaled using information about topography. This is augmented by an independent precipitation dataset – Gridded Estimates of daily and monthly Areal Rainfall for the United Kingdom (CEH-GEAR; Tanguy et al. (2014); Keller et al. (2015)) – along with variables from two global datasets – WFD and CRU TS 3.21 – to produce a comprehensive, observation-based, daily meteorological dataset at 1 km × 1 km spatial resolution.

In order to understand the effect of meteorology on the water cycle, a key variable in hydrological modelling is the atmospheric evaporative demand (AED), which is determined by meteorological variables (Kay et al., 2013). It has been shown that water-resource and hydrological model results are largely driven by how this property is defined and used (Haddeland et al., 2011). The AED can be expressed in several ways, for instance the evaporation from a wet surface, from a well-watered but dry uniform vegetated cover, or from a hypothetical well-watered but dry version of the actual vegetation. Metrics such as the Palmer Drought Severity Index (PDSI; Palmer (1965)) use potential evapotranspiration (PET) as an input while many hydrological models such as Climate and Land use Scenario Simulation in Catchments (CLASSIC; Crooks and Naden (2007)) or Grid-to-Grid (G2G; Bell et al. (2009)), use as input a distinct form of the PET which includes the intercepted water from rainfall (this is described later in the text) which we hereby name PETI. While hydrological models can make use of high resolution topographic information and precipitation datasets, they are often

driven with PET calculated at a coarser resolution (Bell et al., 2011; Bell et al., 2012; Kay et al., 2015). Therefore, we have also created a dataset consisting of estimates of PET and PETI, which can be used to run high-resolution hydrological models (Robinson et al., 2015b).

Other regional studies have created gridded estimates of AED in Austria (Haslinger and Bartsch, 2016) and Australia (Donohue et al., 2010). Regional studies of trends in AED have seen varied results, with increasing AED seen in Romania (Paltineanu et al., 2012), Serbia (Gocic and Trajkovic, 2013), Spain (Vicente-Serrano et al., 2014), some regions of China (Li and Zhou, 2014) and Iran (Azizzadeh and Javan, 2015; Hosseinzadeh Talaee et al., 2013; Tabari et al., 2012), decreasing AED in north east India (Jhajharia et al., 2012) and regions in China (Yin et al., 2009; Song, 2010; Shan et al., 2015; Zhao et al., 2015; Zhang et al., 2015; Lu et al., 2016) and regional variability in Australia (Donohue et al., 2010) and China (Li et al., 2015). In order to understand this variability, it is important to quantify the relative contributions of the changing meteorological variables to trends in AED and regional studies often find different drivers of changing AED (see McVicar et al. (2012) for a review). Relative humidity has been shown to drive AED in the Canary Islands (Vicente-Serrano et al., 2016), wind speed and air temperature were shown to have nearly equal but opposite effects in Australia (Donohue et al., 2010), while in China sunshine hours (Li et al., 2015), wind speed (Yin et al., 2009) or a combination of the two (Lu et al., 2016) have been shown to drive trends. Rudd and Kay (2015) investigated projected changes in PET using a regional climate model, but little has been done to investigate historical trends of AED in the UK.

The objectives of this paper are (i) to evaluate the trends in key meteorological variables in Great Britain over the years 1961-2012; (ii) to evaluate the AED in Great Britain over the same time period; (iii) to investigate the effect of including interception in the formulation of PET called PETI; (iv) to evaluate trends in PET over the time period of interest; and (v) to attribute the trends in PET to trends in meteorological variables. To address these objectives, the paper is structured as follows. Section 2 presents the calculation of the meteorological variables. Section 3 presents the calculation of PET and PETI from the meteorological variables and assesses the difference between PET and PETI. In Section 4 the trends in annual means of the meteorological variables and AED are calculated and the trends in PET are attributed to trends in meteorological variables. In Section 5 the results are discussed and conclusions are presented in Section 6.

2 Calculation of meteorological variables

The meteorological variables included in this new dataset (Robinson et al., 2015a) are daily mean values of air temperature, specific humidity, wind speed, downward longwave (LW) and shortwave (SW) radiation, precipitation and air pressure, plus daily temperature range (Table 1). These variables are important drivers of near-surface conditions, and, for instance, are the full set of variables required to drive the JULES land surface model (LSM) (Best et al., 2011; Clark et al., 2011), as well as other LSMs.

The data were derived primarily from MORECS, which is a long-term gridded dataset starting in 1961 and updated to the present (Thompson et al., 1981; Hough and Jones, 1997). It interpolates five variables from synoptic stations (daily mean values of air temperature, vapour pressure and wind speed, daily hours of bright sunshine and daily total precipitation) to a 40 km × 40 km resolution grid aligned with the Ordnance Survey National Grid. There are currently 270 stations reporting in real time, while a further 170 report the daily readings on a monthly basis, but numbers have varied throughout the run. The algorithm interpolates a varying number of stations (up to nine) for each square, depending on data availability (Hough and Jones, 1997). The interpolation is such that the value in each grid square is the effective measurement of a station positioned at the centre of the square and at the grid square mean elevation, averaged from 00:00 GMT to 00:00 GMT the next day. MORECS is a consistent, quality-controlled time series, which accounts for changing station coverage. The MORECS variables were used to derive the air temperature, specific humidity, wind speed, downward LW and SW radiation and air pressure in the new dataset. The WFD and CRU TS 3.21 datasets were used for surface air pressure and daily temperature range respectively, as they could not be calculated from MORECS. Additionally precipitation was obtained from the CEH-GEAR data, which is a product directly interpolated to 1 km from the station data (Keller et al., 2015).

The spatial coverage of the dataset was determined by the spatial coverage of MORECS, which covers the majority of Great Britain, but excludes some coastal regions and islands at the 1 km scale. For most of these points, the interpolation was extended from the nearest MORECS squares, but some outlying islands (in particular Shetland and the Scilly Isles) were excluded when the entire island was further than 40 km from the nearest MORECS square.

2.1 Air temperature

Air temperature, T_a (K), was derived from the MORECS air temperature. The MORECS air temperature was reduced to mean sea level, using a lapse rate of -0.006 K m^{-1} (Hough and Jones, 1997). A bicubic spline was used to interpolate from 40 km resolution to 1 km resolution, then the temperatures were adjusted to the elevation of each 1 km square using the same lapse rate. The 1 km resolution elevation data used were aggregated from the Integrated Hydrological Digital Terrain Model (IHDTM) – a 50 m resolution digital terrain model (Morris and Flavin, 1990).

2.2 Specific humidity

Specific humidity, q_a (kg kg^{-1}), was derived from the MORECS vapour pressure, which was first reduced to mean sea level, using a lapse rate of -0.025 % m^{-1} (Thompson et al., 1981). The actual lapse rate of humidity will, in general, vary according to atmospheric conditions. However, calculating this would require more detailed information than is available in the input data used. Any method of calculating the variation of specific humidity with height will involve several assumptions, but the method used here is well-established and is used by the Met Office in calculating MORECS (Thompson et al., 1981). The value of the vapour pressure lapse rate is chosen to keep relative humidity constant with altitude, rather than assuming that the specific humidity itself is constant.

A bicubic spline was used to interpolate vapour pressure to 1 km resolution then the values were adjusted to the 1 km resolution elevation using the IHDTM elevations. Finally the specific humidity was calculated, using

$$q_a = \frac{\epsilon e}{p_* - (1-\epsilon)e}, \tag{1}$$

where e is the vapour pressure (Pa) and $\epsilon = 0.622$ is the mass ratio of water to dry air (Gill, 1982). The air pressure, p_*, in this calculation was assumed to have a constant value of 100000 Pa because this was prescribed in the computer code. It would be better to use a varying air pressure, as calculated in Section 2.8, but this makes a negligible difference (of a few percent) to the calculated specific humidity and a constant p_* was retained.

2.3 Downward shortwave radiation

Downward SW radiation, S_d (W m^{-2}), was derived from the MORECS hours of bright sunshine (defined as the total number of hours in a day for which solar irradiation exceeds 120 W m^{-2} (WMO, 2013)). The value calculated is the mean SW radiation over 24 hours. The sunshine hours were used to calculate the cloud cover factor, $C_f = n/N$, where n is the number of hours of bright sunshine in a day, and N is the total number of hours between sunrise and sunset (Marthews et al., 2011). The cloud cover factor was interpolated to 1 km resolution using a bicubic spline. The downward SW solar radiation for a horizontal plane at the Earth's surface was then calculated using the solar angle equations of Iqbal (1983) and a form of the Angstrom-Prescott equation which relates hours of bright sunshine to solar irradiance (Ångström, 1918; Prescott, 1940), with empirical coefficients calculated by Cowley (1978). They vary spatially and seasonally and effectively account for reduction of irradiance with increasing solar zenith angle, as well as implicitly accounting for spatially- and seasonally-varying aerosol effects. However, they do not vary interannually and thus do not explicitly include long-term trends in aerosol concentration.

The downward SW radiation was then corrected for the average inclination and aspect of the surface, assuming that only the direct beam radiation is a function of the inclination and that the diffuse radiation is homogeneous. It was also assumed that the cloud cover is the dominant factor in determining the diffuse fraction (Muneer and Munawwar, 2006). The aspect and inclination were calculated using the IHDTM elevation at 50 m resolution, following the method of Horn (1981), and were then aggregated to 1 km resolution. The top of atmosphere flux for horizontal and inclined surfaces was calculated following Allen et al. (2006) and the ratio used to scale the direct beam radiation.

2.4 Downward longwave radiation

Downward LW radiation, L_d (W m^{-2}), was derived from the 1 km resolution air temperature (Sect. 2.1), vapour pressure (Sect. 2.2) and cloud cover factor (Sect. 2.3). The downward LW radiation for clear sky conditions was calculated as a function of air temperature and precipitable water using the method of Dilley and O'Brien (1998), with precipitable water calculated from air temperature and humidity following Prata (1996). The additional component due to cloud cover was calculated using the equations of Kimball et al. (1982), assuming a constant cloud base height of 1000 m.

2.5 Wind speed

The wind speed at a height of 10 m, u_{10} (m s^{-1}), was derived from the MORECS 10 m wind speed, which were interpolated to 1 km resolution using a bicubic spline and adjusted for topography using a 1 km resolution dataset of mean wind speeds produced by the UK Energy Technology Support Unit (ETSU) (Newton and Burch, 1985; Burch and Ravenscroft, 1992). This used Numerical Objective Analysis Boundary Layer (NOABL) methodology and station wind measurements over the period 1975-84 to produce a map of mean wind speed over the UK. To calculate the topographic correction, the ETSU wind speed was aggregated to 40 km resolution, then the difference between each 1 km value and the corresponding 40 km mean found. This difference was added to the interpolated daily wind speed. In cases where this would result in a negative wind speed, the wind speed was set to zero.

2.6 Precipitation

Precipitation rate, P (kg m^{-2} s^{-1}), is taken from the daily CEH-GEAR dataset (Tanguy et al., 2014; Keller et al., 2015), scaled to the appropriate units. The CEH-GEAR methodology uses natural neighbour interpolation (Gold, 1989) to interpolate synoptic station data to a 1 km resolution gridded daily dataset of the estimated precipitation in 24 hours between 09:00 GMT and 09:00 GMT the next day.

2.7 Daily temperature range

Daily temperature range (DTR), D_T (K), was obtained from the CRU TS 3.21 monthly mean daily temperature range estimates on a 0.5° latitude × 0.5° longitude grid, which is interpolated from monthly climate observations (Harris et al., 2014; Jones and Harris, 2013). There is no standard way to correct DTR for elevation, so these data were reprojected to the 1 km grid with no interpolation and the monthly mean used to populate the daily values in each month. Although DTR is not required in the calculation of AED, it is a required input of the JULES LSM, in order to run at sub-daily timestep.

2.8 Surface air pressure

Surface air pressure, p_* (Pa), was derived from the WFD, an observation-corrected reanalysis product, which provides 3 hourly meteorological data for 1958-2001 on a 0.5° latitude × 0.5° longitude resolution grid (Weedon et al., 2011). Mean monthly values of WFD surface air

245 pressure and air temperature were calculated for each 0.5° grid box over the years 1961-2001.
246 These were reprojected to the 1 km grid with no interpolation, then the lapse rate of air
247 temperature (Sect. 2.1) used to calculate the integral of the hypsometric equation, in order to
248 obtain the air pressure at the elevation of each 1 km grid (Shuttleworth, 2012). The mean
249 monthly values were used to populate the daily values in the full dataset, thus the surface air
250 pressure in the new dataset does not vary interanually, but does vary seasonally. This is
251 reasonable as the trend in surface air pressure in the WFD is negligible (Weedon et al., 2011).

2.9 Spatial and seasonal patterns of meteorological variables

253 Long-term mean values of the meteorological variables were calculated for each 1 km square
254 over the whole dataset (1961-2012) (Fig. 1). Four sub-regions of interest were defined (Fig. 2);
255 three of these regions correspond to nations (England, Wales and Scotland), while the fourth is
256 the 'English lowlands', a subset of England, covering south-central and south-east England,
257 East Anglia and the East Midlands (Folland et al., 2015). Mean-monthly climatologies (Fig. 3)
258 were calculated over the whole of Great Britain (GB), and over these four regions of interest.

259 The maps clearly show the effect of topography on the variables (Fig. 1), with an inverse
260 correlation between elevation and temperature, specific humidity, downward LW radiation and
261 surface air pressure and a positive correlation with wind speed. The precipitation has an east-
262 west gradient due to prevailing weather systems and orography. The fine-scale structure of the
263 downward SW radiation is due to the aspect and elevation of each grid cell, with more spatial
264 variability in areas with more varying terrain. As no topographic correction has been applied to
265 DTR, it varies only on a larger spatial scale. Although specific humidity is inversely
266 proportional to elevation, relative humidity is not, as the saturated specific humidity will also
267 be inversely proportional to elevation due to the decrease in temperature with height.

268 The mean-monthly climatologies (Fig. 3) demonstrate the differences between the regions, with
269 Scotland generally having lower temperatures and more precipitation than the average, and
270 England (particularly the English lowlands) being warmer and drier.

2.10 Validation of meteorology

272 The precipitation dataset, CEH-GEAR, has previously been validated against observations
273 (Keller et al., 2015). Other studies discuss the uncertainties in the CRU TS 3.21 daily
274 temperature range data (Harris et al., 2014) and WFDEI air pressure data (Weedon et al., 2014).

275   For the other variables, the MORECS data set is ultimately derived from the synoptic stations
276   around the UK which represent most of the available observed meteorological data. The only
277   way to validate the gridded meteorology presented here is to compare it to independently
278   observed data, which are available at a few sites where meteorological measurement stations
279   are located. Here we carry out a validation exercise with data from four sites from the UK,
280   which have meteorological measurements available for between 5 and 10 years. Details of the
281   sites and data are in Appendix A. Fig. 4 shows the comparison of data set air temperature with
282   the observed air temperature at each of the four sites. This shows a strong correlation (r^2
283   between 0.94 and 0.97) between the data set and the observations. Fig. 5 shows the mean-
284   monthly climatology calculated from both the data set and from the observations (only for times
285   for which observations were available) and demonstrates that the data set successfully captures
286   the seasonal cycle. This has been repeated for downward SW radiation and for an estimate of
287   the mixing ratio of water vapour, 10 m wind speed and surface air pressure (Appendix A). The
288   air temperature, downward SW radiation and mixing ratio all have high correlations and
289   represent the seasonal cycle well. The wind speed is overestimated by the derived data set at
290   two sites, which is likely to be due to land cover effects. The modelling which produced the
291   ETSU dataset uses topography but not land cover (Burch and Ravenscroft, 1992; Newton and
292   Burch, 1985), so at sites with tall vegetation the wind speed is likely to be less than the modelled
293   value. The air pressure has a low correlation because the data set contains a mean-monthly
294   climatological value. However, the mean bias is low and the RMSE is small, confirming that it
295   is reasonable to use a climatological value in place of daily data.

296 **3   Calculation of potential evapotranspiration (PET)**

297   There are several ways to assess the evaporative demand of the atmosphere. Pan evaporation
298   can be modelled using the Pen-Pan model, or open-water evaporation can be modelled with the
299   Penman equation. However, neither of these account for the fact that in general the evaporation
300   is occurring from a vegetated surface. A widely used model is the Penman-Monteith PET, E_P
301   (mm d^{-1}, equivalent to kg m^{-2} d^{-1}), which is a physically-based formulation of the AED of the
302   atmosphere (Monteith, 1965). It provides an estimate of AED dependent on the atmospheric
303   conditions but allowing for the fact that that the water is evaporating through the surface of
304   leaves and thus the resistance is higher. It is calculated from the daily meteorological variables
305   using the equation

306 $$E_P = \frac{t_d}{\lambda} \frac{\Delta A + \frac{c_p \rho_a}{r_a}(q_s - q_a)}{\Delta + \gamma \left(1 + \frac{r_s}{r_a}\right)} \,,$$ (2)

307 where t_d = 86400 s d^{-1} is the length of a day, λ=2.5×10^6 J kg^{-1} is the latent heat of evaporation,

308 q_s is saturated specific humidity (kg kg^{-1}), Δ is the gradient of saturated specific humidity with

309 respect to temperature (kg kg^{-1} K^{-1}), A is the available energy (W m^{-2}), c_p=1010 J kg^{-1} K^{-1} is the

310 specific heat capacity of air, ρ_a is the density of air (kg m^{-3}), q_a is specific humidity (kg kg^{-1}),

311 γ=0.004 K^{-1} is the psychrometric constant, r_s is stomatal resistance (s m^{-1}) and r_a is aerodynamic

312 resistance (s m^{-1}) (Stewart, 1989).

313 The saturated specific humidity, q_s (kg kg^{-1}), is calculated from saturated vapour pressure, e_s

314 (Pa), using Eq. (1). The saturated vapour pressure is calculated using an empirical fit to air

315 temperature

316 $$e_s = p_s exp \left(\sum_{i=1}^{4} a_i \left(1 - \frac{T_s}{T_a}\right)^i \right) \,,$$ (3)

317 where p_s = 101325 Pa is the steam point pressure, T_s = 373.15 K is the steam point temperature

318 and a=(13.3185, -1.9760, -0.6445, -0.1299) are empirical coefficients (Richards, 1971).

319 The derivative of the saturated specific humidity with respect to temperature, Δ (kg kg^{-1} K^{-1}),

320 is therefore

321 $$\Delta = \frac{T_s}{T_a^2} \frac{p_* q_s}{p_* - (1 - \epsilon)e_s} \sum_{i=1}^{4} i a_i \left(1 - \frac{T_s}{T_a}\right)^{i-1} \,.$$ (4)

322 The available energy, A (W m^{-2}), is the energy balance of the surface,

323 $$A = R_n - G \,,$$ (5)

324 where R_n is the net radiation (W m^{-2}) and G is the soil heat flux (W m^{-2}). The net soil heat flux

325 is negligible at the daily timescale (Allen et al., 1998), so the available energy is equal to the

326 net radiation, such that

327 $$A = (1 - \alpha)S_d + \varepsilon(L_d - \sigma T_*^4) \,,$$ (6)

328 where σ is the Stefan-Boltzmann constant, α is the albedo and ε the emissivity of the surface

329 and T_* is the surface temperature (Shuttleworth, 2012). For this study the surface temperature

330 is approximated by using the air temperature, T_a.

331 The air density, ρ_a (kg m^{-3}), is a function of air pressure and temperature,

332 $\rho_a = \frac{p_*}{rT_a}$, (7)

333 where $r = 287.05$ J kg^{-1} K^{-1} is the gas constant of air.

334 The stomatal and aerodynamic resistances are strongly dependent on land cover due to
335 differences in roughness length and physiological constraints on transpiration of different
336 vegetation types. In addition, the albedo and emissivity are also dependent on the land cover.
337 In order to investigate the effect of meteorology on AED, as distinct from land use effects, the
338 PET was calculated for a single land cover type over the whole of the domain. If necessary, this
339 can be adjusted to give an estimate of PET specific to the local land cover, for example using
340 regression relationships (Crooks and Naden, 2007). As a standard, the Food and Agriculture
341 Organization of the United Nations (FAO) calculate reference crop evaporation for a
342 hypothetical reference crop, which corresponds to a well-watered grass (Allen et al., 1998).
343 Following this, the PET in the current study was calculated for a reference crop of 0.12 m
344 height, with constant stomatal resistance, $r_s = 70.0$ s m^{-1}, an albedo of 0.23 and emissivity of
345 0.92 over the whole of Great Britain. This study therefore neglects the effect of land-use on
346 evaporation, which could be investigated in future by calculating PET for different land surface
347 types, with different coverage for each year of the dataset.

348 Following Allen et al. (1998), the aerodynamic resistance, r_a (s m^{-1}), is a function of the 10 m
349 wind speed

350 $r_a = \frac{278}{u_{10}}$. (8)

351 Thus the PET is a function of six of the meteorological variables: air temperature, specific
352 humidity, downward LW and SW radiation, wind speed and surface air pressure.

353 To explore the role of the different meteorological variables in the AED, it is helpful to split
354 the radiative component (the first part of the numerator in Equation 2) from the wind component
355 (the second part). Formally, this is defined as follows (Doorenbos, 1977):

356 The radiative component, E_{PR},

357 $E_{PR} = \frac{t_d}{\lambda} \frac{\Delta A}{\Delta + \gamma\left(1 + \frac{r_s}{r_a}\right)}$, (9)

358 and the aerodynamic component, E_{PA},

359 $E_{PA} = \frac{t_d}{\lambda} \frac{\frac{c_p \rho_a}{r_a}(q_s - q_a)}{\Delta + \gamma\left(1 + \frac{r_s}{r_a}\right)}$, (10)

360   such that $E_P=E_{PR}+E_{PA}$.

3.1   Potential evapotranspiration with interception (PETI)

When rain falls, water is intercepted by the canopy. The evaporation of this water is not constrained by stomatal resistance but is subject to the same aerodynamic resistance as transpiration (Shuttleworth, 2012). At the same time, transpiration is inhibited in a wet canopy. Suppression of transpiration is well observed both by comparing eddy-covariance fluxes and observations of sap flow (Kume et al., 2006; Moors, 2012), and by observing stomatal and photosynthesis response to wetting (Ishibashi and Terashima, 1995). For plants which have at least some of their stomata on the upper surface of the leaves, this can be due to water directly blocking the stomata. However, in GB most plants have stomata only on the underside of the leaves, so the transpiration is inhibited by other mechanisms.

Physically, the suppression may simply be due to the fact that energy is used in evaporating the intercepted water, so less is available for transpiration (Bosveld and Bouten, 2003) or that the increased humidity of the air, due to evaporation of intercepted water, causes the stomata to close (Lange et al., 1971). It may also be due to the presence of water causing stomatal closure through physiological reactions, which can be observed even when the stomata are on the underside of a leaf and the water is lying on the upper side (Ishibashi and Terashima, 1995).

In the short term after a rain event, potential water losses due to evaporation may be underestimated if only potential transpiration is calculated, and therefore overall rates underestimated. As transpiration is inhibited over the wet fraction of the canopy (Ward and Robinson, 2000) , the PET over a grid box will be a linear combination of the potential interception and potential transpiration, each weighted by the fraction of the canopy that is wet or dry. This can be accounted for by introducing an interception term to the calculation of PET, giving PETI. This is modelled as an interception store, which is (partially) filled by rainfall, proportionally inhibiting the transpiration. As the interception store dries, the relative contribution of interception is decreased and the transpiration increases. This correction is applied on days with precipitation, while on days without precipitation, the potential is equal to the PET defined in Eq. 2. Although an unconventional definition of PET, a similar interception correction is applied to the PET provided at 40 km resolution by MORECS (Thompson et al., 1981) which is used widely by hydrologists.

390   This method implicitly assumes that the water is liquid, however snow lying on the canopy will

391   also inhibit transpiration, and will be depleted by melting as well as by sublimation. The rates

392   may be slower, and the snow may stay on the canopy for longer than one day. However, the

393   difference of accounting for canopy snow as distinct from canopy water will have a small effect

394   on large-scale averages, as the number of lying snow days in GB is relatively low, and they

395   occur during winter when the PET is very small.

396   The PETI is a weighted sum of the PET, E_P, (as calculated in Eq 2.) and potential interception,

397   E_I, which is calculated by substituting zero stomatal resistance, $r_s=0$ s m^{-1}, into Eq. 2. To

398   calculate the relative proportions of interception and transpiration, it is assumed that the wet

399   fraction of the canopy is proportional to the amount of water in the interception store. The

400   interception store, S_I (kg m^{-2}), decreases through the day according to an exponential dry down

401   (Rutter et al., 1971), such that

402     $$S_I(t) = S_o e^{-\frac{E_I}{S_{tot}}t} ,\qquad\qquad(11)$$

403   where E_I is the potential interception, S_{tot} is the total capacity of the interception store (kg m^{-2}),

404   S_0 is the precipitation that is intercepted by the canopy (kg m^{-2}) and t is the time (in days) since

405   a rain event. The total capacity of the interception store is calculated following Best et al.

406   (2011), such that

407     $$S_{tot} = 0.5 + 0.05\Lambda ,\qquad\qquad(12)$$

408   where Λ is the leaf area index (LAI); for the FAO standard grass land cover the LAI is 2.88

409   (Allen et al., 1998). The fraction of precipitation intercepted by the canopy is found also

410   following Best et al. (2011), assuming that precipitation lasts for an average of 3 hours.

411   The wet fraction of the canopy, C_{wet}, is proportional to the store size, such that

412     $$C_{wet}(t) = \frac{S(t)}{S_{tot}} .\qquad\qquad(13)$$

413   The total PETI is the sum of the interception from the wet canopy and the transpiration from

414   the dry canopy,

415     $$E_{PI}(t) = E_I C_{wet}(t) + E_P\left(1 - C_{wet}(t)\right) .\qquad\qquad(14)$$

416   This is integrated over one day to find the total PETI, E_{PI} (mm d^{-1}), to be

$$E_{PI} = S_0 \left(1 - e^{-\frac{E_I}{S_{tot}}} \right) + E_P \left(1 - \frac{S_0}{E_I} \left(1 - e^{-\frac{E_I}{S_{tot}}} \right) \right).$$

(15)

The PETI is a function of the same six meteorological variables as the PET, plus the precipitation.

3.2 Spatial and seasonal patterns of PET and PETI

Both PET and PETI have a distinct gradient from low in the north-west to high in the south-east, and they are both inversely proportional to the elevation (Fig. 6), reflecting the spatial patterns of the meteorological variables. The PETI is 8 % higher than the PET overall but this difference is larger in the north and west, where precipitation rates, and therefore interception, are higher (Fig. 6). In Scotland, the higher interception and lower AED mean that this increase is a larger proportion of the total, with the mean PETI being 11 % larger than the PET (in some areas the difference is more than 25%). In the English lowlands the difference is smaller, at 6 %, but this is a more water limited region where hydrological modelling can be sensitive to even relatively small adjustments to PET (Kay et al., 2013).

The seasonal climatology of both PET and PETI follow the meteorology (Fig. 7), with high values in the summer and low in the winter. Although the relative difference peaks in winter, the absolute difference between PET and PETI is bimodal, with a peak in March and a smaller peak in October (September in Scotland) (Fig. 7), because in winter the overall AED is low, while in summer the amount of precipitation is low, so the interception correction is small. The seasonal cycle of PET is driven predominantly by the radiative component, which has a much stronger seasonality than the aerodynamic component (Fig. 8).

On a monthly or annual timescale, the ratio of PET to precipitation is an indicator of the wet- or dryness of a region (Oldekop, 1911; Andréassian et al., 2016). Low values of PET relative to precipitation indicate wet regions, where evaporation is demand-limited, while high values indicate dry, water-limited regions. In the wetter regions (Scotland, Wales) mean-monthly PET and PETI (Fig. 7) are on average lower than the mean-monthly precipitation (Fig. 3) throughout the year, while in drier regions (England, English lowlands) the mean PET and PETI are higher than the precipitation for much of the summer, highlighting the regions' susceptibility to hydrological drought (Folland et al., 2015).

4 Decadal trends

4.1 Meteorological Variables

Annual means of the meteorological variables (Fig. 9) and the PET and PETI (Fig. 10) were calculated for each region. The trends in these annual means were calculated using linear regression; the significance (P value) and 95% confidence intervals (CI) of the slope are calculated specifically allowing for the non-zero lag-1 autocorrelation, to account for possible correlations between adjacent data points (Zwiers and von Storch, 1995; von Storch and Zwiers, 1999). In addition, seasonal means were calculated, with the four seasons defined to be Winter (December-February), Spring (March-May), Summer (June-August) and Autumn (September-November), and trends in these means were also found. The trends can be seen in Table 2.

The trends in the annual and seasonal means for all regions are plotted in Fig. 11; trends that are statistically significant at the 5% level are plotted with solid error bars, those that are not significant are plotted with dashed lines. The analysis was repeated for each pixel in the 1 km resolution dataset; maps of these rates of change can be seen in Appendix B.

There was a statistically significant trend in air temperature in all regions (except in winter), which agrees with recent trends in the Hadley Centre Central England Temperature (HadCET) dataset (Parker and Horton, 2005) and in temperature records for Scotland (Jenkins et al., 2008) as well as in the CRUTEM4 dataset (Jones et al., 2012). An increase in winter precipitation in Scotland is seen in the current dataset, which leads to a statistically significant increase in the annual mean precipitation of GB. However, all other regions and seasons have no statistically significant trends in precipitation. Long term observations show that there has been little trend in annual precipitation, but a change in seasonality with wetting winters and drying summers since records began, although with little change over the past 50 years (Jenkins et al., 2008). The statistically significant decline in wind speed in all regions is consistent with the results of McVicar et al. (2012) and Vautard et al. (2010), who report decreasing wind speeds in the northern hemisphere over the late 20th century.

4.2 Potential Evapotranspiration

The trends of the meteorological variables are interesting in their own right. But for hydrology, it is the impact that the trends have on evaporation that matters and that depends on their combination, which can be expressed through PET.

476 The regional trends of annual mean PET and PETI can be seen in Table 2, and the trends in the

477 annual and seasonal means of PET, PETI, and the radiative and aerodynamic components of

478 PET are plotted in Fig. 12 for all regions. Maps of the trends can be seen in Appendix B. The

479 trend in the radiative component of PET is positive over the whole of GB. However, the trend

480 in the aerodynamic component varies; for much of Wales, Scotland and northern England, it is

481 not significant, or is slightly negative, while in south-east England and north-west Scotland it

482 is positive. This leads to a positive trend in PET over much of GB, but no significant trend in

483 southern Scotland and northern England. There is a statistically significant increase in annual

484 PET in all regions except Wales; the GB trend (0.021 ± 0.021 mm d^{-1} decade^{-1}) is equivalent to

485 an increase of 0.11 ± 0.11 mm d^{-1} (8.3 ± 8.1 % of the long term mean) over the whole dataset.

486 Increases in PETI are only statistically significant in England (0.023 ± 0.023 mm d^{-1} decade^{-1})

487 and English lowlands (0.028 ± 0.025 mm d^{-1} decade^{-1}), where the increases over the whole

488 dataset are 0.12 ± 0.12 mm d^{-1} (8.0 ± 8.0 % of the long term mean) and 0.15 ± 0.13 mm d^{-1} (9.7 ± 8.8

489 % of the long term mean) respectively. There is a difference in trend between different seasons.

490 In winter, summer and autumn there are no statistically significant trends in PET or PETI, other

491 than the English lowlands in autumn, but the spring is markedly different, with very significant

492 trends ($P<0.0005$) in all regions. The GB spring trends in PET (0.043 ± 0.019 mm d^{-1} decade^{-1})

493 and PETI (0.038 ± 0.018 mm d^{-1} decade^{-1}) are equivalent to an increase of 0.22 ± 0.10 mm d^{-1}

494 (13.8 ± 6.2 % of the long-term spring mean) and 0.20 ± 0.09 mm d^{-1} (11.2 ± 5.3 % of the long-term

495 spring mean) over the length of the dataset respectively. The radiative component of PET has

496 similarly significant trends in spring, while the aerodynamic component has no significant

497 trends in any season (Fig. 12), indicating that the trend in PET is due to the increasing radiative

498 component.

499 There are few studies of long-term trends in AED in the UK. MORECS provides an estimate

500 of Penman-Monteith PET with interception correction calculated directly from the 40 km

501 resolution meteorological data (Hough and Jones, 1997; Thompson et al., 1981), and increases

502 can be seen over the dataset (Rodda and Marsh, 2011). But as the PET and PETI in the current

503 dataset are ultimately calculated using the same meteorological data (albeit by different

504 methods), it is not unexpected that similar trends should be seen. Site-based studies suggest an

505 increase over recent decades (Burt and Shahgedanova, 1998; Crane and Hudson, 1997), but it

506 is difficult to separate climate-driven trends from local land-use trends. A global review paper

507 (McVicar et al., 2012) identified a trend of decreasing AED in the northern hemisphere, driven

508 by decreasing wind speeds, however they also reported significant local variations on trends in

pan evaporation, including the increasing trend observed by Stanhill and Möller (2008) at a site in England after 1968. Matsoukas et al. (2011) identified a statistically significant increase in PET in several regions of the globe, including southern England, between 1983 and 2008, attributing it predominantly to an increase in the radiative component of PET, due to global brightening. However, these results were obtained using reanalysis data, which is limited in its ability to capture trends in wind speed. This limitation has been documented in both northern (Pryor et al., 2009) and southern (McVicar et al., 2008) hemispheres.

Regional changes in actual evaporative losses can be estimated indirectly using regional precipitation and runoff or river flow. Using a combination of observations and modelling, Marsh and Dixon (2012) identified an increase in evaporative losses in Great Britain from 1961-2011. Hannaford and Buys (2012) note seasonal and regional differences in trends in observed river flow, suggesting that decreasing spring flows in the English lowlands are indicative of increasing AED. However, changing evaporative losses can also be due to changing supply through precipitation, so it is important to formally attribute the trends in PET to changing climate, in order to understand changing evapotranspiration.

4.3   Attribution of trends in potential evapotranspiration

In order to attribute changes in PET to changes in climate, the rate of change of PET, dE_p/dt (mm d^{-1} decade^{-1}), can be calculated as a function of the rate of change of each variable (Roderick et al., 2007),

$$\frac{dE_P}{dt} = \frac{dE_P}{dT_a}\frac{dT_a}{dt} + \frac{dE_P}{dq_a}\frac{dq_a}{dt} + \frac{dE_P}{du_{10}}\frac{du_{10}}{dt} + \frac{dE_P}{dL_d}\frac{dL_d}{dt} + \frac{dE_P}{dS_d}\frac{dS_d}{dt} \ . \tag{16}$$

Note that we exclude the surface air pressure, because this dataset uses a mean-monthly climatology as the interannual variability of air pressure is negligible. The derivative of the PET with respect to each of the meteorological variables can be found analytically (Appendix C). The derivatives are calculated from the daily meteorological data at 1 km resolution. Substituting the slopes of the linear regressions of the gridded annual means (Appendix B) for the rate of change of each variable with time, and the overall time-average of the derivatives of PET with respect to the meteorological variables, the contribution of each variable to the rate of change of PET can be calculated at 1 km resolution. These are then averaged over the regions of interest. The same can also be applied to the radiative and aerodynamic components independently.

539 Note that this can also be applied to the regional means of the derivatives of PET and the trends

540 in the meteorological variables. The results are compared in Table 3 and the two approaches

541 are consistent. For the regional analysis, we also quote the 95% CI. However, for the gridded

542 values, there is such high spatial coherence that combining the 95% CI over the region results

543 in unreasonably constrained results. We therefore use the more conservative CI obtained from

544 the regional analysis. Also note that this method assumes that the rate of change of the variables

545 with respect to time is constant over the whole dataset (and thus the product of the means is

546 equal to the mean of the products), and indeed this is how it is often applied (Donohue et al.,

547 2010; Lu et al., 2016). The effect of this assumption was investigated by repeating the analysis

548 with seasonal trends and means, but this makes negligible difference to the results.

549 Fig. 13 shows the contribution of each meteorological variable to the rate of change of the

550 annual mean PET and to the radiative and aerodynamic components and compares the total

551 attributed trend to that obtained by linear regression. The percentage contribution is in Table 4,

552 calculated as a fraction of the fitted trend. The final columns shows the total attributed trend as

553 a percentage of the fitted trend, to demonstrate the success of the attribution at recovering the

554 fitted trends. For the PET trend and for the trend in the radiative component, these values

555 generally sum to the linear regression to within a few percent. However, for the aerodynamic

556 component, the fitted trend is very small (an order of magnitude smaller than the PET and

557 radiative component trends), and much smaller than the statistical uncertainty. This means that

558 there can be a large and/or negative percentage difference between the attributed and fitted

559 trends, even when the absolute difference is negligible.

560 The largest overall contribution to the rate of change of PET comes from increasing air

561 temperature, which has the effect of increasing the aerodynamic component (as it makes the air

562 more able to hold water), but it decreases the radiative component (due to increasing outgoing

563 LW radiation). However, the decrease due to increasing specific humidity largely cancels this

564 increase in the aerodynamic component. Overall the next largest increases are caused by

565 increasing downward SW radiation, particularly in the English regions in the spring, as it

566 increases the radiative component of PET. However, in Scotland and Wales, the increasing

567 downward LW radiation is also important. Finally, the decreasing wind speed has the effect of

568 increasing the radiative component, but decreasing the aerodynamic component, so overall it

569 tends to cause a decrease in PET.

570 Since the increasing air temperature and downward LW and SW radiation have the effect of
571 increasing PET, but the increasing specific humidity and decreasing wind speed tend to
572 decrease it, then the overall trend is positive, but smaller than the trend due to air temperature
573 alone.

574 **5 Discussion**

575 These high resolution datasets provide insight into the effect of the changing climate of Great
576 Britain on AED over the past five decades. There have been significant climatic trends in the
577 UK since 1961; in particular rising air temperature and specific humidity, decreasing wind
578 speed and decreasing cloudiness. Although some are positive and some negative, these
579 meteorological trends combine to give statistically significant trends in PET.

580 Wind speeds have decreased more significantly in the west than the east, and show a consistent
581 decrease across seasons. Contrary to Donohue et al. (2010) and McVicar et al. (2012), this study
582 finds that the change in wind speed of the late 20th and early 21st centuries has had a negligible
583 influence on PET over the period of study. However, the previous studies were concerned with
584 open-water Penman evaporation, which has a simpler (proportional) dependence on wind speed
585 than the Penman-Monteith PET considered here (Schymanski and Or, 2015).

586 The air temperature trend in this study of 0.21 ± 0.15 K decade^{-1} in GB is consistent with
587 observed global and regional trends (Hartmann et al., 2013; Jenkins et al., 2008). The
588 temperature trend is responsible for a large contribution to the trend in PET, although the large
589 negative contribution from the specific humidity (as well as a small negative contribution from
590 wind speed) means that the overall trend is smaller than the temperature trend alone.

591 Although the contribution is smaller than that of air temperature, the trends in LW radiation in
592 these datasets contribute to between 15% and 28% of the trends in PET and between 27% and
593 46% or the trends in the radiative component. Observations of LW radiation are often uncertain,
594 but the trend in this dataset, although small, is consistent with observed trends (Wang and Liang,
595 2009), as well as with trends in the WFDEI bias-corrected reanalysis product (Weedon et al.,
596 2014).

597 Increasing solar radiation has been shown to increase spring and annual AED, contributing to
598 between 18% and 50% of the fitted trend in annual PET, and to between 43% and 53% of the
599 fitted trend in spring PET. Two main mechanisms can be responsible for changing solar
600 radiation – changing cloud cover and changing aerosol concentrations. Changing aerosol

601 emissions have been shown to have had a significant effect on solar radiation in the 20th century.
602 In Europe, global dimming due to increased aerosol concentrations peaked around 1980,
603 followed by global brightening as aerosol concentrations decreased (Wild, 2009). Observations
604 of changing continental runoff and river flow in Europe over the 20th century have been
605 attributed to changing aerosol concentrations, via their effect on solar radiation, and thus AED
606 (Gedney et al., 2014).

607 In this study we use the duration of bright sunshine to calculate the solar radiation, using
608 empirical coefficients which do not vary with year, so aerosol effects are not explicitly included.
609 The coefficients used in this study to convert sunshine hours to radiation fluxes were
610 empirically derived in 1978; the derivation used data from the decade 1966-75, as this period
611 was identified to be before reductions in aerosol emissions had begun to significantly alter
612 observed solar radiation (Cowley, 1978). Despite this, the trend in SW radiation in the current
613 dataset from 1979 onwards (1.4 ± 1.4 W m^{-2} decade^{-1}) is consistent, within uncertainties, with
614 that seen over GB in the WFDEI data (0.9 ± 1.1 W m^{-2} decade^{-1}), which is bias-corrected to
615 observations and includes explicit aerosol effects (Weedon et al., 2014).

616 It has been suggested that aerosol effects also implicitly affect sunshine duration since in
617 polluted areas, there will be fewer hours above the official 'sunshine hours' threshold of 120
618 Wm^{-2} (Helmes and Jaenicke, 1986). Several regional studies have shown trends in sunshine
619 hours that are consistent with the periods of dimming and brightening across the globe (eg
620 Liley, 2009; Sanchez-Lorenzo et al., 2009; Sanchez-Lorenzo et al., 2008; Stanhill and Cohen,
621 2005), and several have attempted to quantify the relative contribution of trends in cloud cover
622 and aerosol loading (e.g. Sanchez-Lorenzo and Wild (2012) in Switzerland, see Sanchez-
623 Romero et al. (2014) for a review). Therefore, it may be that some of the brightening trend seen
624 in the current dataset is due to the implicit signal of aerosol trends in the MORECS sunshine
625 duration, although this is likely to be small compared to the effects of changing cloud cover.

626 The trends in the MORECS sunshine duration used in this study are consistent with changing
627 weather patterns which may be attributed to the Atlantic Multidecadal Oscillation (AMO). The
628 AMO has been shown to cause a decrease in spring precipitation (and therefore cloud cover) in
629 northern Europe over recent decades (Sutton and Dong, 2012), and the trend in MORECS
630 sunshine hours is dominated by an increase in the spring mean. This has also been seen in
631 Europe-wide sunshine hours data (Sanchez-Lorenzo et al., 2008). On the other hand, the effect
632 of changing aerosols on sunshine hours is expected to be largest in the winter (Sanchez-Lorenzo

633   et al., 2008). However, it would not be possible to directly identify either of these effects on the
634   sunshine duration without access to longer data records.

635   The inclusion of explicit aerosol effects in the coefficients of the Angstrom-Prescott equation
636   would be expected to reduce the positive trend in AED in the first two decades of the dataset,
637   and increase it after 1980. Gedney et al. (2014) attribute a decrease in European solar radiation
638   of 10 W m^{-2} between the periods 1901-10 and 1974-80, and an increase of 4 W m^{-2} from 1974-
639   84 to1990-99 to changing aerosol contributions. Applying these trends to the current dataset,
640   with a turning point at 1980, would double the overall increase in solar radiation in Great
641   Britain, which would lead to a 40 % increase in the overall trend in PET. So, if this effect were
642   to be included, it would confirm the results found in this paper.

643   Trends in temperature and cloud cover in the UK are expected to continue into the coming
644   decades, with precipitation expected to increase in the winter but decrease in the summer
645   (Murphy et al., 2009). Therefore it is likely that AED will increase, increasing water stress in
646   the summer when precipitation is lower and potentially affecting water resources, agriculture
647   and biodiversity. This has been demonstrated for southern England and Wales by Rudd and
648   Kay (2015), who calculated present and future PET using high-resolution RCM output and
649   include the effects of CO_2 on stomatal opening.

650   The current study is concerned only with the effects of changing climate on AED and has
651   assumed a constant bulk canopy resistance throughout. However, plants are expected to react
652   to increased CO_2 in the atmosphere by closing stomata and limiting the exchange of gases,
653   including water (Kruijt et al., 2008), and observed changes in runoff have been attributed to this
654   effect (Gedney et al., 2006; Gedney et al., 2014). It is possible that the resulting change of
655   canopy resistance could partially offset the increased atmospheric demand (Rudd and Kay,
656   2015) and may impact runoff (Gedney et al., 2006; Prudhomme et al., 2014), but further studies
657   would be required to quantify this.

6   Conclusion

659   This paper has presented a unique high-resolution observation-based dataset of meteorological
660   variables and AED in Great Britain since 1961. Key trends in the meteorological variables are
661   (i) increasing air temperature and specific humidity, consistent with global temperature trends;
662   (ii) increasing solar radiation, particularly in the spring, consistent with changes in aerosol
663   emissions and weather patterns in recent decades; (iii) decreasing wind speed, consistent with
664   observations of global stilling; and (iv) increasing precipitation, driven by increasing winter

precipitation in Scotland. The meteorological variables were used to evaluate AED in Great Britain via calculation of PET and PETI. It has been demonstrated that including the interception component in the calculation of PETI gives a mean estimate that is overall 8% larger than PET alone, with strong seasonality and spatial variation of the difference. PET was found to be increasing by 0.021 ± 0.021 mm d^{-1} decade^{-1} over the study period. With the interception component included, the trend in PETI is weaker, and over GB is not significant at the 5% level. The trend in PET was analytically attributed to the trends in the meteorological variables, and it was found that the dominant effect was that increasing air temperature was driving increasing PET. This is largely compensated by the associated increase in specific humidity, as the water cycle is intensified under climate change and by decreasing wind speed. However, the PET increase is also driven by increasing solar radiation, particularly in the spring.

In addition to providing meteorological data for analysis, the meteorological variables provided are sufficient to run LSMs and hydrological models. The high spatial (1 km) and temporal (daily) resolution will allow this dataset to be used to study the effects of climate on physical and biological systems at a range of scales, from local to national.

Data Access

The data can be downloaded from the Environmental Information Platform at the Centre for Ecology & Hydrology. The meteorological variables can be found at

https://catalogue.ceh.ac.uk/documents/80887755-1426-4dab-a4a6-250919d5020c,

while the PET and PETI can be accessed at

https://catalogue.ceh.ac.uk/documents/d329f4d6-95ba-4134-b77a-a377e0755653.

Author contribution

EB, JF and DBC designed the study. JF, ACR, DBC and ELR developed code to create meteorological data. ELR created the PET and PETI. ELR and EB analysed trends. ELR, EB, ACR and DBC wrote the manuscript.

Acknowledgements

The meteorological variables presented are based largely on GB meteorological data under licence from the Met Office, and those organisations contributing to this national dataset (including the Met Office, Environment Agency, Scottish Environment Protection Agency (SEPA) and Natural Resources Wales) are gratefully acknowledged. The CRU TS 3.21 daily

696   temperature range data were created by the University of East Anglia Climatic Research Unit,

697   and the WFD air pressure data were created as part of the EU FP6 project WATCH (Contract

698   036946). Collection of flux data was funded by EU FP4 EuroFlux (Griffin Forest); EU FP5

699   CarboEuroFlux (Griffin Forest); EU FP5 GreenGrass (Easter Bush); EU FP6 CarboEuropeIP

700   (Alice Holt , Griffin Forest, Auchencorth Moss, Easter Bush); EU FP6 IMECC (Griffin

701   Forest); the Forestry Commission (Alice Holt); the Natural Environment Research Council,

702   UK (Auchencorth Moss, Easter Bush).

703   Thanks to Nicola Gedney and Graham Weedon for useful discussions.

704   This work was partially funded by the Natural Environment Research Council in the

705   Changing Water Cycle programme: NERC Reference: NE/I006087/1.

706

Appendix A: Data validation

Meteorological data were downloaded from the European Fluxes Database Cluster (http://gaia.agraria.unitus.it) for four sites positioned around Great Britain. Two were woodland sites (Alice Holt (Wilkinson et al., 2012; Heinemeyer et al., 2012) and Griffin Forest (Clement, 2003)), while two had grass and crop cover (Auchencorth Moss (Billett et al., 2004) and Easter Bush (Gilmanov et al., 2007; Soussana et al., 2007)). Table A1 gives details of the data used. The data are provided as half-hourly measurements, which were used to create daily means, where full daily data coverage was available. The daily means of the observed data were compared to the daily data from the grid square containing the site and the Pearson correlation (r^2), mean bias and root mean square error (RMSE) were calculated. For each site, monthly means were calculated where the full month had available data, then a climatology calculated from available months. The same values were calculated from the relevant grid squares, using only time periods for which observed data were available.

Fig. A1 shows the comparison of the data set downward SW radiation against daily mean air temperature observed at the four sites. Fig. A2 shows the mean-monthly climatology of the daily values. The observed values of the mixing ratio of water vapour in air were compared with values calculated from the meteorological dataset, using the equation

$$r_w = q_a \left(\frac{m_a}{m_w} \right)$$

where m_a is the molecular mass of dry air and m_w is the molecular mass of water. The comparisons are shown in Figs. A3 and A4.

Table A2 shows the r^2, mean bias and RMSE for each of the variables included in the validation exercise. The correlations indicate a good relationship between the dataset variables and the independent observations at the sites, while the mean-monthly climatologies demonstrate that the data represent the seasonal cycle well.

Appendix B: Trend maps

Fig. B1 shows the rate of change of each of the meteorological variables at the 1 km resolution, while Fig. B2 shows the rate of change of the PET, PETI, and the two components of PET at the same resolution. This shows that the regional trends are consistent with spatial variation and are not dominated by individual extreme points.

Appendix C: Derivatives of PET

737 The wind speed affects the PET through the aerodynamic resistance. The derivative with respect

738 to wind speed is

739
$$\frac{\partial E_P}{\partial u_{10}} = \frac{(\Delta+\gamma)E_{PA} - \gamma\frac{r_s}{r_a}E_{PR}}{u_{10}\left(\Delta+\gamma\left(1+\frac{r_s}{r_a}\right)\right)} \ . \tag{C1}$$

740 The downward LW and SW radiation affect PET through the net radiation, and the derivatives

741 are

742
$$\frac{\partial E_P}{\partial L_d} = E_{PR}\frac{\epsilon}{R_n} \tag{C2}$$

743
$$\frac{\partial E_P}{\partial S_d} = E_{PR}\frac{(1-\alpha)}{R_n} \ . \tag{C3}$$

744 The derivative of PET with respect to specific humidity is

745
$$\frac{\partial E_P}{\partial q_a} = \frac{E_{PA}}{q_a-q_s} \ . \tag{C4}$$

746 The air temperature affects PET through the saturated specific humidity and its derivative, the

747 net radiation and the air density, so that the derivative of PET with respect to air temperature is

748
$$\frac{\partial E_P}{\partial T_a} = E_{PR}\left(\frac{\gamma\left(1+\frac{r_s}{r_a}\right)}{T_a^2\left(\Delta+\gamma\left(1+\frac{r_s}{r_a}\right)\right)}\left[T_{sp}\left(\sum_{i=1}^4 ia_iT_r^{i-1} + \frac{\sum_{i=1}^4 ia_iT_r^{i-1}}{\sum_{i=1}^4 i(i-1)a_iT_r^{i-2}} + \frac{2(1-\varepsilon)\sum_{i=1}^4 ia_iT_r^{i-1}q_s}{\varepsilon}\right) - \right.$$

749
$$\left. 2T_a\right] - \frac{4\epsilon\sigma T_a^4}{R_n}\right) + E_{PA}\left(\frac{\Delta}{q_s-q} - \frac{1}{T_a} - \frac{\Delta}{T_a^2\left(\Delta+\gamma\left(1+\frac{r_s}{r_a}\right)\right)}\left[T_{sp}\left(\sum_{i=1}^4 ia_iT_r^{i-1} + \frac{\sum_{i=1}^4 ia_iT_r^{i-1}}{\sum_{i=1}^4 i(i-1)a_iT_r^{i-2}} + \right.\right.$$

750
$$\left.\left.\frac{2(1-\varepsilon)\sum_{i=1}^4 ia_iT_r^{i-1}q_s}{\varepsilon}\right) - 2T_a\right]\right) \ . \tag{C5}$$

7 References

752 Allen, R. G., Pereira, L. S., Raes, D., and Smith, M.: Crop evapotranspiration - Guidelines for
753 computing crop water requirements, Food and Agriculture Organization of the United
754 Nations, Rome, Italy, FAO Irrigation and Drainage Paper, 1998.

755 Allen, R. G., Trezza, R., and Tasumi, M.: Analytical integrated functions for daily solar
756 radiation on slopes, Agr Forest Meteorol, 139, 55-73, doi:10.1016/j.agrformet.2006.05.012,
757 2006.

758 Andréassian, V., Mander, Ü., and Pae, T.: The Budyko hypothesis before Budyko: The
759 hydrological legacy of Evald Oldekop, Journal of Hydrology, 535, 386-391,
760 http://dx.doi.org/10.1016/j.jhydrol.2016.02.002, 2016.

761 Ångström, A.: A study of the radiation of the atmosphere, Smithsonian Miscellaneous
762 Collections, 65, 159-161, 1918.

763 Azizzadeh, M., and Javan, K.: Analyzing Trends in Reference Evapotranspiration in
764 Northwest Part of Iran, Journal of Ecological Engineering, 16, 1-12,
765 10.12911/22998993/1853, 2015.

766 Baldocchi, D., Valentini, R., Running, S., Oechel, W., and Dahlman, R.: Strategies for
767 measuring and modelling carbon dioxide and water vapour fluxes over terrestrial ecosystems,
768 Global Change Biology, 2, 159-168, doi:10.1111/j.1365-2486.1996.tb00069.x, 1996.

769 Bell, V. A., Kay, A. L., Jones, R. G., Moore, R. J., and Reynard, N. S.: Use of soil data in a
770 grid-based hydrological model to estimate spatial variation in changing flood risk across the
771 UK, Journal of Hydrology, 377, 335-350, doi:10.1016/j.jhydrol.2009.08.031, 2009.

772 Bell, V. A., Gedney, N., Kay, A. L., Smith, R. N. B., Jones, R. G., and Moore, R. J.:
773 Estimating Potential Evaporation from Vegetated Surfaces for Water Management Impact
774 Assessments Using Climate Model Output, Journal of Hydrometeorology, 12, 1127-1136,
775 doi:10.1175/2011jhm1379.1, 2011.

776 Bell, V. A., Kay, A. L., Cole, S. J., Jones, R. G., Moore, R. J., and Reynard, N. S.: How might
777 climate change affect river flows across the Thames Basin? An area-wide analysis using the
778 UKCP09 Regional Climate Model ensemble, Journal of Hydrology, 442-443, 89-104,
779 doi:10.1016/j.jhydrol.2012.04.001, 2012.

780 Bellamy, P. H., Loveland, P. J., Bradley, R. I., Lark, R. M., and Kirk, G. J.: Carbon losses
781 from all soils across England and Wales 1978-2003, Nature, 437, 245-248,
782 doi:10.1038/nature04038, 2005.

783 Berry, P. M., Dawson, T. P., Harrison, P. A., and Pearson, R. G.: Modelling potential impacts
784 of climate change on the bioclimatic envelope of species in Britain and Ireland, Global Ecol
785 Biogeogr, 11, 453-462, doi:10.1046/j.1466-822x.2002.00304.x, 2002.

786 Best, M. J., Pryor, M., Clark, D. B., Rooney, G. G., Essery, R. L. H., Ménard, C. B., Edwards,
787 J. M., Hendry, M. A., Porson, A., Gedney, N., Mercado, L. M., Sitch, S., Blyth, E., Boucher,
788 O., Cox, P. M., Grimmond, C. S. B., and Harding, R. J.: The Joint UK Land Environment
789 Simulator (JULES), model description – Part 1: Energy and water fluxes, Geoscientific Model
790 Development, 4, 677-699, doi:10.5194/gmd-4-677-2011, 2011.

791 Billett, M. F., Palmer, S. M., Hope, D., Deacon, C., Storeton-West, R., Hargreaves, K. J.,
792 Flechard, C., and Fowler, D.: Linking land-atmosphere-stream carbon fluxes in a lowland
793 peatland system, Global Biogeochemical Cycles, 18, n/a-n/a, 10.1029/2003gb002058, 2004.

794 Bosveld, F. C., and Bouten, W.: Evaluating a Model of Evaporation and Transpiration with
795 Observations in a Partially Wet Douglas-Fir Forest, Boundary-Layer Meteorology, 108, 365-
796 396, 10.1023/a:1024148707239, 2003.

797 Burch, S. F., and Ravenscroft, F.: Computer modelling of the UK wind energy resource: Final
798 overview report., AEA Industrial Technology, 1992.

799 Burt, T. P., and Shahgedanova, M.: An historical record of evaporation losses since 1815
800 calculated using long-term observations from the Radcliffe Meteorological Station, Oxford,
801 England, Journal of Hydrology, 205, 101-111, doi:10.1016/S0022-1694(97)00143-1, 1998.

802 Clark, D. B., Mercado, L. M., Sitch, S., Jones, C. D., Gedney, N., Best, M. J., Pryor, M.,
803 Rooney, G. G., Essery, R. L. H., Blyth, E., Boucher, O., Harding, R. J., Huntingford, C., and
804 Cox, P. M.: The Joint UK Land Environment Simulator (JULES), model description – Part 2:

Carbon fluxes and vegetation dynamics, Geoscientific Model Development, 4, 701-722, doi:10.5194/gmd-4-701-2011, 2011.

Clement, R. M., J.B.; Jarvis, P.G.: Net carbon productivity of Sitka Spruce forest in Scotland, Scottish Forestry, 5-10, 2003.

Cowley, J. P.: The distribution over Great Britain of global solar irradiation on a horizontal surface, Meteorological Magazine, 107, 357-372, 1978.

Crane, S. B., and Hudson, J. A.: The impact of site factors and climate variability on the calculation of potential evaporation at Moel Cynnedd, Plynlimon, Hydrol. Earth Syst. Sci., 1, 429-445, doi:10.5194/hess-1-429-1997, 1997.

Crooks, S. M., and Naden, P. S.: CLASSIC: a semi-distributed rainfall-runoff modelling system, Hydrol. Earth Syst. Sci., 11, 516-531, doi:10.5194/hess-11-516-2007, 2007.

Crooks, S. M., and Kay, A. L.: Simulation of river flow in the Thames over 120 years: Evidence of change in rainfall-runoff response?, Journal of Hydrology: Regional Studies, 4, Part B, 172-195, doi:10.1016/j.ejrh.2015.05.014, 2015.

Dilley, A. C., and O'Brien, D. M.: Estimating downward clear sky long-wave irradiance at the surface from screen temperature and precipitable water, Quarterly Journal of the Royal Meteorological Society, 124, 1391-1401, doi:10.1256/Smsqj.54902, 1998.

Donohue, R. J., McVicar, T. R., and Roderick, M. L.: Assessing the ability of potential evaporation formulations to capture the dynamics in evaporative demand within a changing climate, Journal of Hydrology, 386, 186-197, doi:10.1016/j.jhydrol.2010.03.020, 2010.

Doorenbos, J. a. P., W. O.: Crop water requirements. FAO Irrigation and Drainage Paper 24., FAO, Rome, Italy, 1977.

Evans, N., Baierl, A., Semenov, M. A., Gladders, P., and Fitt, B. D.: Range and severity of a plant disease increased by global warming, Journal of the Royal Society, Interface / the Royal Society, 5, 525-531, doi:10.1098/rsif.2007.1136, 2008.

FAO/IIASA/ISRIC/ISS-CAS/JRC: Harmonized World Soil Database, 2012.

Fleig, A. K., Tallaksen, L. M., James, P., Hisdal, H., and Stahl, K.: Attribution of European precipitation and temperature trends to changes in synoptic circulation, Hydrology and Earth System Sciences, 19, 3093-3107, 10.5194/hess-19-3093-2015, 2015.

Folland, C. K., Hannaford, J., Bloomfield, J. P., Kendon, M., Svensson, C., Marchant, B. P., Prior, J., and Wallace, E.: Multi-annual droughts in the English Lowlands: a review of their characteristics and climate drivers in the winter half-year, Hydrology and Earth System Sciences, 19, 2353-2375, doi:10.5194/hess-19-2353-2015, 2015.

Gedney, N., Cox, P. M., Betts, R. A., Boucher, O., Huntingford, C., and Stott, P. A.: Detection of a direct carbon dioxide effect in continental river runoff records, Nature, 439, 835-838, doi:10.1038/nature04504, 2006.

Gedney, N., Huntingford, C., Weedon, G. P., Bellouin, N., Boucher, O., and Cox, P. M.: Detection of solar dimming and brightening effects on Northern Hemisphere river flow, Nature Geoscience, 7, 796-800, doi:10.1038/ngeo2263, 2014.

Gill, A. E.: Atmosphere-ocean Dynamics, Academic Press, San Diego, California, USA, 1982.

846   Gilmanov, T. G., Soussana, J. F., Aires, L., Allard, V., Ammann, C., Balzarolo, M., Barcza,
847   Z., Bernhofer, C., Campbell, C. L., Cernusca, A., Cescatti, A., Clifton-Brown, J., Dirks, B. O.
848   M., Dore, S., Eugster, W., Fuhrer, J., Gimeno, C., Gruenwald, T., Haszpra, L., Hensen, A.,
849   Ibrom, A., Jacobs, A. F. G., Jones, M. B., Lanigan, G., Laurila, T., Lohila, A., G.Manca,
850   Marcolla, B., Nagy, Z., Pilegaard, K., Pinter, K., Pio, C., Raschi, A., Rogiers, N., Sanz, M. J.,
851   Stefani, P., Sutton, M., Tuba, Z., Valentini, R., Williams, M. L., and Wohlfahrt, G.:
852   Partitioning European grassland net ecosystem CO2 exchange into gross primary productivity
853   and ecosystem respiration using light response function analysis, Agriculture, Ecosystems &
854   Environment, 121, 93-120, 10.1016/j.agee.2006.12.008, 2007.

855   Gocic, M., and Trajkovic, S.: Analysis of trends in reference evapotranspiration data in a
856   humid climate, Hydrological Sciences Journal, 59, 165-180, 10.1080/02626667.2013.798659,
857   2013.

858   Gold, C. M.: Surface interpolation, spatial adjacency and GIS, in: Three Dimensional
859   Applications in Geographical Information Systems, edited by: Raper, J., Taylor and Francis,
860   London, 1989.

861   Haddeland, I., Clark, D. B., Franssen, W., Ludwig, F., Voß, F., Arnell, N. W., Bertrand, N.,
862   Best, M., Folwell, S., Gerten, D., Gomes, S., Gosling, S. N., Hagemann, S., Hanasaki, N.,
863   Harding, R., Heinke, J., Kabat, P., Koirala, S., Oki, T., Polcher, J., Stacke, T., Viterbo, P.,
864   Weedon, G. P., and Yeh, P.: Multimodel Estimate of the Global Terrestrial Water Balance:
865   Setup and First Results, Journal of Hydrometeorology, 12, 869-884, 10.1175/2011jhm1324.1,
866   2011.

867   Hannaford, J., and Buys, G.: Trends in seasonal river flow regimes in the UK, Journal of
868   Hydrology, 475, 158-174, doi:10.1016/j.jhydrol.2012.09.044, 2012.

869   Hannaford, J.: Climate-driven changes in UK river flows: A review of the evidence, Progress
870   in Physical Geography, 39, 29-48, doi:10.1177/0309133314536755, 2015.

871   Harris, I., Jones, P. D., Osborn, T. J., and Lister, D. H.: Updated high-resolution grids of
872   monthly climatic observations - the CRU TS3.10 Dataset, International Journal of
873   Climatology, 34, 623-642, doi:10.1002/Joc.3711, 2014.

874   Hartmann, D. L., Klein Tank, A. M. G., Rusticucci, M., Alexander, L. V., Brönnimann, S.,
875   Charabi, Y., Dentener, F. J., Dlugokencky, E. J., Easterling, D. R., Kaplan, A., Soden, B. J.,
876   Thorne, P. W., Wild, M., and Zhai, P. M.: Observations: Atmosphere and Surface, in: Climate
877   Change 2013: The Physical Science Basis. Contribution of Working Group I to the Fifth
878   Assessment Report of the Intergovernmental Panel on Climate Change, edited by: Stocker, T.
879   F., Qin, D., Plattner, G.-K., Tignor, M., Allen, S. K., Boschung, J., Nauels, A., Xia, Y., Bex,
880   V., and Midgley, P. M., Cambridge University Press, Cambridge, United Kingdom and New
881   York, NY, USA, 159–254, 2013.

882   Haslinger, K., and Bartsch, A.: Creating long-term gridded fields of reference
883   evapotranspiration in Alpine terrain based on a recalibrated Hargreaves method, Hydrology
884   and Earth System Sciences, 20, 1211-1223, 10.5194/hess-20-1211-2016, 2016.

885   Heinemeyer, A., Wilkinson, M., Vargas, R., Subke, J. A., Casella, E., Morison, J. I. L., and
886   Ineson, P.: Exploring the "overflow tap" theory: linking forest soil CO_2 fluxes
887   and individual mycorrhizosphere components to photosynthesis, Biogeosciences, 9, 79-95,
888   10.5194/bg-9-79-2012, 2012.

889   Helmes, L., and Jaenicke, R.: Atmospheric turbidity determined from sunshine records,
890   Journal of Aerosol Science, 17, 261-263, doi:10.1016/0021-8502(86)90080-7, 1986.

891 Hickling, R., Roy, D. B., Hill, J. K., Fox, R., and Thomas, C. D.: The distributions of a wide
892 range of taxonomic groups are expanding polewards, Global Change Biology, 12, 450-455,
893 doi:10.1111/j.1365-2486.2006.01116.x, 2006.

894 Horn, B. K. P.: Hill Shading and the Reflectance Map, P Ieee, 69, 14-47,
895 doi:10.1109/Proc.1981.11918, 1981.

896 Hosseinzadeh Talaee, P., Shifteh Some'e, B., and Sobhan Ardakani, S.: Time trend and
897 change point of reference evapotranspiration over Iran, Theoretical and Applied Climatology,
898 116, 639-647, 10.1007/s00704-013-0978-x, 2013.

899 Hough, M. N., and Jones, R. J. A.: The United Kingdom Meteorological Office rainfall and
900 evaporation calculation system: MORECS version 2.0-an overview, Hydrology and Earth
901 System Sciences, 1, 227-239, doi:10.5194/hess-1-227-1997, 1997.

902 IPCC: Climate Change 2013: The Physical Science Basis. Contribution of Working Group I
903 to the Fifth Assessment Report of the Intergovernmental Panel on Climate Change,
904 Cambridge University Press, Cambridge, United Kingdom and New York, NY, USA, 1535
905 pp., 2013.

906 IPCC: Climate Change 2014: Impacts, Adaptation, and Vulnerability. Part A: Global and
907 Sectoral Aspects. Contribution of Working Group II to the Fifth Assessment Report of the
908 Intergovernmental Panel on Climate Change [Field, C.B., V.R. Barros, D.J. Dokken, K.J.
909 Mach, M.D. Mastrandrea, T.E. Bilir, M. Chatterjee, K.L. Ebi, Y.O. Estrada, R.C. Genova, B.
910 Girma, E.S. Kissel, A.N. Levy, S. MacCracken, P.R. Mastrandrea, and L.L. White (eds.)],
911 Cambridge University Press, Cambridge, United Kingdom and New York, NY, USA, 1132
912 pp., 2014a.

913 IPCC: Climate Change 2014: Impacts, Adaptation, and Vulnerability. Part B: Regional
914 Aspects. Contribution of Working Group II to the Fifth Assessment Report of the
915 Intergovernmental Panel on Climate Change [Barros, V.R., C.B. Field, D.J. Dokken, M.D.
916 Mastrandrea, K.J. Mach, T.E. Bilir, M. Chatterjee, K.L. Ebi, Y.O. Estrada, R.C. Genova, B.
917 Girma, E.S. Kissel, A.N. Levy, S. MacCracken, P.R. Mastrandrea, and L.L. White (eds.)],
918 Cambridge University Press, Cambridge, United Kingdom and New York, NY, USA, 688
919 pp., 2014b.

920 Iqbal, M.: An introduction to solar radiation, Academic Press, London, 1983.

921 Ishibashi, M., and Terashima, I.: Effects of continuous leaf wetness on photosynthesis:
922 adverse aspects of rainfall, Plant, Cell & Environment, 18, 431-438, 10.1111/j.1365-
923 3040.1995.tb00377.x, 1995.

924 Jenkins, G. J., Perry, M. C., and Prior, M. J.: The climate of the United Kingdom and recent
925 trends, Met Office Hadley Centre, Exeter, UK, 2008.

926 Jhajharia, D., Dinpashoh, Y., Kahya, E., Singh, V. P., and Fakheri-Fard, A.: Trends in
927 reference evapotranspiration in the humid region of northeast India, Hydrological Processes,
928 26, 421-435, 10.1002/hyp.8140, 2012.

929 Jones, P. D., Lister, D. H., Osborn, T. J., Harpham, C., Salmon, M., and Morice, C. P.:
930 Hemispheric and large-scale land-surface air temperature variations: An extensive revision
931 and an update to 2010, Journal of Geophysical Research: Atmospheres, 117, n/a-n/a,
932 doi:10.1029/2011JD017139, 2012.

933 Jones, P. D., and Harris, I.: CRU TS3.21: Climatic Research Unit (CRU) Time-Series (TS)
934 Version 3.21 of High Resolution Gridded Data of Month-by-month Variation in Climate (Jan.

1901- Dec. 2012). University of East Anglia Climatic Research Unit, doi:10.5285/D0E1585D-3417-485F-87AE-4FCECF10A992, 2013.

Kay, A. L., Bell, V. A., Blyth, E. M., Crooks, S. M., Davies, H. N., and Reynard, N. S.: A hydrological perspective on evaporation: historical trends and future projections in Britain, Journal of Water and Climate Change, 4, 193, doi:10.2166/wcc.2013.014, 2013.

Kay, A. L., Rudd, A. C., Davies, H. N., Kendon, E. J., and Jones, R. G.: Use of very high resolution climate model data for hydrological modelling: baseline performance and future flood changes, Climatic Change, doi:10.1007/s10584-015-1455-6, 2015.

Keller, V. D. J., Tanguy, M., Prosdocimi, I., Terry, J. A., Hitt, O., Cole, S. J., Fry, M., Morris, D. G., and Dixon, H.: CEH-GEAR: 1 km resolution daily and monthly areal rainfall estimates for the UK for hydrological and other applications, Earth Syst. Sci. Data, 7, 143-155, doi:10.5194/essd-7-143-2015, 2015.

Kimball, B. A., Idso, S. B., and Aase, J. K.: A Model of Thermal-Radiation from Partly Cloudy and Overcast Skies, Water Resources Research, 18, 931-936, doi:10.1029/Wr018i004p00931, 1982.

Kruijt, B., Witte, J.-P. M., Jacobs, C. M. J., and Kroon, T.: Effects of rising atmospheric CO2 on evapotranspiration and soil moisture: A practical approach for the Netherlands, Journal of Hydrology, 349, 257-267, doi:10.1016/j.jhydrol.2007.10.052, 2008.

Kume, T., Kuraji, K., Yoshifuji, N., Morooka, T., Sawano, S., Chong, L., and Suzuki, M.: Estimation of canopy drying time after rainfall using sap flow measurements in an emergent tree in a lowland mixed-dipterocarp forest in Sarawak, Malaysia, Hydrological Processes, 20, 565-578, 10.1002/hyp.5924, 2006.

Lange, O. L., Lösch, R., Schulze, E.-D., and Kappen, L.: Responses of stomata to changes in humidity, Planta, 100, 76-86, 10.1007/bf00386887, 1971.

Li, B., Chen, F., and Guo, H.: Regional complexity in trends of potential evapotranspiration and its driving factors in the Upper Mekong River Basin, Quaternary International, 380-381, 83-94, 10.1016/j.quaint.2014.12.052, 2015.

Li, Y., and Zhou, M.: Trends in Dryness Index Based on Potential Evapotranspiration and Precipitation over 1961–2099 in Xinjiang, China, Advances in Meteorology, 2014, 1-15, 10.1155/2014/548230, 2014.

Liley, J. B.: New Zealand dimming and brightening, Journal of Geophysical Research, 114, doi:10.1029/2008jd011401, 2009.

Lu, X., Bai, H., and Mu, X.: Explaining the evaporation paradox in Jiangxi Province of China: Spatial distribution and temporal trends in potential evapotranspiration of Jiangxi Province from 1961 to 2013, International Soil and Water Conservation Research, 4, 45-51, 10.1016/j.iswcr.2016.02.004, 2016.

Marsh, T., and Dixon, H.: The UK water balance – how much has it changed in a warming world?, 01-05, doi:10.7558/bhs.2012.ns32, 2012.

Marthews, T. R., Malhi, Y., and Iwata, H.: Calculating downward longwave radiation under clear and cloudy conditions over a tropical lowland forest site: an evaluation of model schemes for hourly data, Theoretical and Applied Climatology, 107, 461-477, 10.1007/s00704-011-0486-9, 2011.

977 Matsoukas, C., Benas, N., Hatzianastassiou, N., Pavlakis, K. G., Kanakidou, M., and
978 Vardavas, I.: Potential evaporation trends over land between 1983–2008: driven by radiative
979 fluxes or vapour-pressure deficit?, Atmospheric Chemistry and Physics, 11, 7601-7616,
980 doi:10.5194/acp-11-7601-2011, 2011.

981 McVicar, T. R., Van Niel, T. G., Li, L. T., Roderick, M. L., Rayner, D. P., Ricciardulli, L.,
982 and Donohue, R. J.: Wind speed climatology and trends for Australia, 1975–2006: Capturing
983 the stilling phenomenon and comparison with near-surface reanalysis output, Geophysical
984 Research Letters, 35, n/a-n/a, 10.1029/2008GL035627, 2008.

985 McVicar, T. R., Roderick, M. L., Donohue, R. J., Li, L. T., Van Niel, T. G., Thomas, A.,
986 Grieser, J., Jhajharia, D., Himri, Y., Mahowald, N. M., Mescherskaya, A. V., Kruger, A. C.,
987 Rehman, S., and Dinpashoh, Y.: Global review and synthesis of trends in observed terrestrial
988 near-surface wind speeds: Implications for evaporation, Journal of Hydrology, 416, 182-205,
989 doi:10.1016/j.jhydrol.2011.10.024, 2012.

990 Monteith, J. L.: Evaporation and environment, in: 19th Symposia of the Society for
991 Experimental Biology, University Press, Cambridge, 1965.

992 Moors, E.: Water Use of Forests in the Netherlands, PhD, Vrije Universiteit, Amsterdam, the
993 Netherlands, 2012.

994 Morris, D. G., and Flavin, R. W.: A digital terrain model for hydrology., Proceedings of the
995 4th International Symposium on Spatial Data Handling, 1, 250-262, 1990.

996 Morton, D., Rowland, C., Wood, C., Meek, L., Marston, C., Smith, G., Wadsworth, R., and
997 Simpson, I. C.: Final Report for LCM2007 - the new UK land cover map, NERC/Centre for
998 Ecology & Hydrology 11/07 (CEH Project Number: C03259), 2011.

999 Muneer, T., and Munawwar, S.: Potential for improvement in estimation of solar diffuse
1000 irradiance, Energ Convers Manage, 47, 68-86, doi:10.1016/j.enconman.2005.03.015, 2006.

1001 Murphy, J. M., Sexton, D. M. H., Jenkins, G. J., Boorman, P. M., Booth, B. B. B., Brown, C.
1002 C., Clark, R. T., Collins, M., Harris, G. R., Kendon, E. J., Betts, R. A., Brown, S. J., Howard,
1003 T. P., Humphrey, K. A., McCarthy, M. P., McDonald, R. E., Stephens, A., Wallace, C.,
1004 Warren, R., Wilby, R., and Wood, R. A.: UK Climate Projections Science Report: Climate
1005 change projections, Met Office Hadley Centre, Exeter, 2009.

1006 Newton, K., and Burch, S. F.: Estimation of the UK wind energy resource using computer
1007 modelling techniques and map data, Energy Technology Support Unit, 50, 1985.

1008 Norton, L. R., Maskell, L. C., Smart, S. S., Dunbar, M. J., Emmett, B. A., Carey, P. D.,
1009 Williams, P., Crowe, A., Chandler, K., Scott, W. A., and Wood, C. M.: Measuring stock and
1010 change in the GB countryside for policy--key findings and developments from the
1011 Countryside Survey 2007 field survey, Journal of environmental management, 113, 117-127,
1012 doi:10.1016/j.jenvman.2012.07.030, 2012.

1013 Oldekop, E.: Evaporation from the surface of river basins, in: Collection of the Works of
1014 Students of the Meteorological Observatory, University of Tartu-Jurjew-Dorpat, Tartu,
1015 Estonia, 209, 1911.

1016 Palmer, W. C.: Meteorological Drought. Res. Paper No.45, Dept. of Commerce, Washington,
1017 D.C., 1965.

1018 Paltineanu, C., Chitu, E., and Mateescu, E.: New trends for reference evapotranspiration and
1019 climatic water deficit, International Agrophysics, 26, 10.2478/v10247-012-0023-9, 2012.

1020 Parker, D., and Horton, B.: Uncertainties in central England temperature 1878-2003 and some
1021 improvements to the maximum and minimum series, International Journal of Climatology, 25,
1022 1173-1188, doi:10.1002/joc.1190, 2005.

1023 Pocock, M. J., Roy, H. E., Preston, C. D., and Roy, D. B.: The Biological Records Centre in
1024 the United Kingdom: a pioneer of citizen science., Biological Journal of the Linnean Society,
1025 doi:10.1111/bij.12548, 2015.

1026 Prata, A. J.: A new long-wave formula for estimating downward clear-sky radiation at the
1027 surface, Quarterly Journal of the Royal Meteorological Society, 122, 1127-1151,
1028 doi:10.1002/qj.49712253306, 1996.

1029 Prescott, J. A.: Evaporation from a water surface in relation to solar radiation, Transaction of
1030 the Royal Society of South Australia, 64, 114-125, 1940.

1031 Prudhomme, C., Giuntoli, I., Robinson, E. L., Clark, D. B., Arnell, N. W., Dankers, R.,
1032 Fekete, B. M., Franssen, W., Gerten, D., Gosling, S. N., Hagemann, S., Hannah, D. M., Kim,
1033 H., Masaki, Y., Satoh, Y., Stacke, T., Wada, Y., and Wisser, D.: Hydrological droughts in the
1034 21st century, hotspots and uncertainties from a global multimodel ensemble experiment,
1035 Proceedings of the National Academy of Sciences, 111, 3262-3267,
1036 doi:10.1073/pnas.1222473110, 2014.

1037 Pryor, S. C., Barthelmie, R. J., Young, D. T., Takle, E. S., Arritt, R. W., Flory, D., Gutowski,
1038 W. J., Nunes, A., and Roads, J.: Wind speed trends over the contiguous United States, Journal
1039 of Geophysical Research: Atmospheres, 114, n/a-n/a, 10.1029/2008JD011416, 2009.

1040 Reynolds, B., Chamberlain, P. M., Poskitt, J., Woods, C., Scott, W. A., Rowe, E. C.,
1041 Robinson, D. A., Frogbrook, Z. L., Keith, A. M., Henrys, P. A., Black, H. I. J., and Emmett,
1042 B. A.: Countryside Survey: National "Soil Change" 1978–2007 for Topsoils in Great
1043 Britain—Acidity, Carbon, and Total Nitrogen Status, Vadose Zone Journal, 12, 0,
1044 doi:10.2136/vzj2012.0114, 2013.

1045 Richards, J. M.: A simple expression for the saturation vapour pressure of water in the range
1046 −50 to 140°C, Journal of Physics D: Applied Physics, 4, L15, 1971.

1047 Robinson, E. L., Blyth, E., Clark, D. B., Finch, J., and Rudd, A. C.: Climate hydrology and
1048 ecology research support system meteorology dataset for Great Britain (1961-2012) [CHESS-
1049 met], NERC-Environmental Information Data Centre, 2015a.

1050 Robinson, E. L., Blyth, E., Clark, D. B., Finch, J., and Rudd, A. C.: Climate hydrology and
1051 ecology research support system potential evapotranspiration dataset for Great Britain (1961-
1052 2012) [CHESS-PE], NERC-Environmental Information Data Centre, 2015b.

1053 Rodda, J. C., and Marsh, T. J.: The 1975-76 Drought - a contemporary and retrospective
1054 review, Wallingford, UK, 2011.

1055 Roderick, M. L., Rotstayn, L. D., Farquhar, G. D., and Hobbins, M. T.: On the attribution of
1056 changing pan evaporation, Geophysical Research Letters, 34, 10.1029/2007gl031166, 2007.

1057 Rudd, A. C., and Kay, A. L.: Use of very high resolution climate model data for hydrological
1058 modelling: estimation of potential evaporation, Hydrology Research, doi:
1059 10.2166/nh.2015.028, 2015.

1060 Rutter, A. J., Kershaw, K. A., Robins, P. C., and Morton, A. J.: A predictive model of rainfall
1061 interception in forests, 1. Derivation of the model from observations in a plantation of
1062 Corsican pine, Agricultural Meteorology, 9, 367-384, doi:10.1016/0002-1571(71)90034-3,
1063 1971.

1064 Sanchez-Lorenzo, A., Calbó, J., and Martin-Vide, J.: Spatial and Temporal Trends in
1065 Sunshine Duration over Western Europe (1938–2004), Journal of Climate, 21, 6089-6098,
1066 doi:10.1175/2008jcli2442.1, 2008.

1067 Sanchez-Lorenzo, A., Calbó, J., Brunetti, M., and Deser, C.: Dimming/brightening over the
1068 Iberian Peninsula: Trends in sunshine duration and cloud cover and their relations with
1069 atmospheric circulation, Journal of Geophysical Research, 114, doi:10.1029/2008jd011394,
1070 2009.

1071 Sanchez-Lorenzo, A., and Wild, M.: Decadal variations in estimated surface solar radiation
1072 over Switzerland since the late 19th century, Atmospheric Chemistry and Physics, 12, 8635-
1073 8644, doi:10.5194/acp-12-8635-2012, 2012.

1074 Sanchez-Romero, A., Sanchez-Lorenzo, A., Calbó, J., González, J. A., and Azorin-Molina,
1075 C.: The signal of aerosol-induced changes in sunshine duration records: A review of the
1076 evidence, Journal of Geophysical Research: Atmospheres, 119, 4657-4673,
1077 doi:10.1002/2013JD021393, 2014.

1078 Schymanski, S. J., and Or, D.: Wind effects on leaf transpiration challenge the concept of
1079 "potential evaporation", Proceedings of the International Association of Hydrological
1080 Sciences, 371, 99-107, 10.5194/piahs-371-99-2015, 2015.

1081 Shan, N., Shi, Z., Yang, X., Zhang, X., Guo, H., Zhang, B., and Zhang, Z.: Trends in potential
1082 evapotranspiration from 1960 to 2013 for a desertification-prone region of China,
1083 International Journal of Climatology, n/a-n/a, 10.1002/joc.4566, 2015.

1084 Sheffield, J., Goteti, G., and Wood, E. F.: Development of a 50-Year High-Resolution Global
1085 Dataset of Meteorological Forcings for Land Surface Modeling, Journal of Climate, 19, 3088-
1086 3111, doi:10.1175/JCLI3790.1, 2006.

1087 Shuttleworth, W. J.: Terrestrial Hydrometeorology, John Wiley & Sons, Ltd, 2012.

1088 Song, Z. W. Z., H. L. ; Snyder, R. L. ;Anderson, F. E. ;Chen, F. : Distribution and Trends in
1089 Reference Evapotranspiration in the North China Plain, Journal of Irrigation and Drainage
1090 Engineering, 136, 240-247, doi:10.1061/(ASCE)IR.1943-4774.0000175, 2010.

1091 Soussana, J. F., Allard, V., Pilegaard, K., Ambus, P., Amman, C., Campbell, C., Ceschia, E.,
1092 Clifton-Brown, J., Czobel, S., Domingues, R., Flechard, C., Fuhrer, J., Hensen, A., Horvath,
1093 L., Jones, M., Kasper, G., Martin, C., Nagy, Z., Neftel, A., Raschi, A., Baronti, S., Rees, R.
1094 M., Skiba, U., Stefani, P., Manca, G., Sutton, M., Tuba, Z., and Valentini, R.: Full accounting
1095 of the greenhouse gas (CO2, N2O, CH4) budget of nine European grassland sites,
1096 Agriculture, Ecosystems & Environment, 121, 121-134, 10.1016/j.agee.2006.12.022, 2007.

1097 Stanhill, G., and Cohen, S.: Solar Radiation Changes in the United States during the
1098 Twentieth Century: Evidence from Sunshine Duration Measurements, Journal of Climate, 18,
1099 1503-1512, doi:10.1175/JCLI3354.1, 2005.

1100 Stanhill, G., and Möller, M.: Evaporative climate change in the British Isles, International
1101 Journal of Climatology, 28, 1127-1137, doi:10.1002/joc.1619, 2008.

1102 Stewart, J. B.: On the use of the Penman-Monteith equation for determining areal
1103 evapotranspiration, in: Estimation of Areal Evapotranspiration (Proceedings of a workshop
1104 held at Vancouver, B.C., Canada, August 1987). edited by: Black, T. A. S., D. L.; Novak, M.
1105 D.; Price, D. T., IAHS, Wallingford, Oxfordshire, UK, 1989.

1106 Sutton, R. T., and Dong, B.: Atlantic Ocean influence on a shift in European climate in the
1107 1990s, Nature Geosci, 5, 788-792, doi:10.1038/ngeo1595, 2012.

1108   Tabari, H., Nikbakht, J., and Hosseinzadeh Talaee, P.: Identification of Trend in Reference
1109   Evapotranspiration Series with Serial Dependence in Iran, Water Resources Management, 26,
1110   2219-2232, 10.1007/s11269-012-0011-7, 2012.

1111   Tanguy, M., Dixon, H., Prosdocimi, I., Morris, D. G., and Keller, V. D. J.: Gridded estimates
1112   of daily and monthly areal rainfall for the United Kingdom (1890-2012) [CEH-GEAR],
1113   NERC Environmental Information Data Centre, doi:10.5285/5dc179dc-f692-49ba-9326-
1114   a6893a503f6e, 2014.

1115   Thackeray, S. J., Sparks, T. H., Frederiksen, M., Burthe, S., Bacon, P. J., Bell, J. R., Botham,
1116   M. S., Brereton, T. M., Bright, P. W., Carvalho, L., Clutton-Brock, T., Dawson, A., Edwards,
1117   M., Elliott, J. M., Harrington, R., Johns, D., Jones, I. D., Jones, J. T., Leech, D. I., Roy, D. B.,
1118   Scott, W. A., Smith, M., Smithers, R. J., Winfield, I. J., and Wanless, S.: Trophic level
1119   asynchrony in rates of phenological change for marine, freshwater and terrestrial
1120   environments, Global Change Biology, 16, 3304-3313, doi:10.1111/j.1365-
1121   2486.2010.02165.x, 2010.

1122   Thompson, N., Barrie, I. A., and Ayles, M.: The Meteorological Office rainfall and
1123   evaporation calculation system: MORECS, Meteorological Office, Bracknell, 1981.

1124   Vautard, R., Cattiaux, J., Yiou, P., Thepaut, J. N., and Ciais, P.: Northern Hemisphere
1125   atmospheric stilling partly attributed to an increase in surface roughness, Nature Geoscience,
1126   3, 756-761, doi:10.1038/Ngeo979, 2010.

1127   Vicente-Serrano, S. M., Azorin-Molina, C., Sanchez-Lorenzo, A., Revuelto, J., López-
1128   Moreno, J. I., González-Hidalgo, J. C., Moran-Tejeda, E., and Espejo, F.: Reference
1129   evapotranspiration variability and trends in Spain, 1961–2011, Global and Planetary Change,
1130   121, 26-40, 10.1016/j.gloplacha.2014.06.005, 2014.

1131   Vicente-Serrano, S. M., Azorin-Molina, C., Sanchez-Lorenzo, A., El Kenawy, A., Martín-
1132   Hernández, N., Peña-Gallardo, M., Beguería, S., and Tomas-Burguera, M.: Recent changes
1133   and drivers of the atmospheric evaporative demand in the Canary Islands, Hydrology and
1134   Earth System Sciences Discussions, 1-35, 10.5194/hess-2016-15, 2016.

1135   Vincent, L. A., Zhang, X., Brown, R. D., Feng, Y., Mekis, E., Milewska, E. J., Wan, H., and
1136   Wang, X. L.: Observed Trends in Canada's Climate and Influence of Low-Frequency
1137   Variability Modes, Journal of Climate, 28, 4545-4560, 10.1175/jcli-d-14-00697.1, 2015.

1138   von Storch, H., and Zwiers, F. W.: Statistical analysis in climate research, Cambridge
1139   University Press, Cambridge ; New York, x, 484 p. pp., 1999.

1140   Wang, K., and Liang, S.: Global atmospheric downward longwave radiation over land surface
1141   under all-sky conditions from 1973 to 2008, Journal of Geophysical Research, 114,
1142   doi:10.1029/2009jd011800, 2009.

1143   Ward, R. C., and Robinson, M.: Principles of Hydrology, McGraw Hill, 2000.

1144   Watts, G., Battarbee, R. W., Bloomfield, J. P., Crossman, J., Daccache, A., Durance, I.,
1145   Elliott, J. A., Garner, G., Hannaford, J., Hannah, D. M., Hess, T., Jackson, C. R., Kay, A. L.,
1146   Kernan, M., Knox, J., Mackay, J., Monteith, D. T., Ormerod, S. J., Rance, J., Stuart, M. E.,
1147   Wade, A. J., Wade, S. D., Weatherhead, K., Whitehead, P. G., and Wilby, R. L.: Climate
1148   change and water in the UK - past changes and future prospects, Progress in Physical
1149   Geography, 39, 6-28, doi:10.1177/0309133314542957, 2015.

1150   Weedon, G. P., Gomes, S., Viterbo, P., Shuttleworth, W. J., Blyth, E., Osterle, H., Adam, J.
1151   C., Bellouin, N., Boucher, O., and Best, M.: Creation of the WATCH Forcing Data and Its

1152   Use to Assess Global and Regional Reference Crop Evaporation over Land during the
1153   Twentieth Century, Journal of Hydrometeorology, 12, 823-848, doi:10.1175/2011jhm1369.1,
1154   2011.

1155   Weedon, G. P., Balsamo, G., Bellouin, N., Gomes, S., Best, M. J., and Viterbo, P.: The
1156   WFDEI meteorological forcing data set: WATCH Forcing Data methodology applied to
1157   ERA-Interim reanalysis data, Water Resources Research, 50, 7505-7514,
1158   doi:10.1002/2014WR015638, 2014.

1159   Wild, M.: Global dimming and brightening: A review, Journal of Geophysical Research, 114,
1160   doi:10.1029/2008jd011470, 2009.

1161   Wilkinson, M., Eaton, E. L., Broadmeadow, M. S. J., and Morison, J. I. L.: Inter-annual
1162   variation of carbon uptake by a plantation oak woodland in south-eastern England,
1163   Biogeosciences, 9, 5373-5389, 10.5194/bg-9-5373-2012, 2012.

1164   WMO: Manual on the Global Observing System, Secretariat of the World Meteorological
1165   Organization, Geneva, Switzerland, 2013.

1166   Wood, C. M., Smart, S. M., and Bunce, R. G. H.: Woodland survey of Great Britain 1971–
1167   2001, Earth System Science Data Discussions, 8, 259-277, doi:10.5194/essdd-8-259-2015,
1168   2015.

1169   Yin, Y., Wu, S., Chen, G., and Dai, E.: Attribution analyses of potential evapotranspiration
1170   changes in China since the 1960s, Theoretical and Applied Climatology, 101, 19-28,
1171   10.1007/s00704-009-0197-7, 2009.

1172   Zhang, K.-x., Pan, S.-m., Zhang, W., Xu, Y.-h., Cao, L.-g., Hao, Y.-p., and Wang, Y.:
1173   Influence of climate change on reference evapotranspiration and aridity index and their
1174   temporal-spatial variations in the Yellow River Basin, China, from 1961 to 2012, Quaternary
1175   International, 380-381, 75-82, 10.1016/j.quaint.2014.12.037, 2015.

1176   Zhao, J., Xu, Z.-x., Zuo, D.-p., and Wang, X.-m.: Temporal variations of reference
1177   evapotranspiration and its sensitivity to meteorological factors in Heihe River Basin, China,
1178   Water Science and Engineering, 8, 1-8, 10.1016/j.wse.2015.01.004, 2015.

1179   Zwiers, F. W., and von Storch, H.: Taking Serial-Correlation into Account in Tests of the
1180   Mean, Journal of Climate, 8, 336-351, doi:10.1175/1520-
1181   0442(1995)008<0336:Tsciai>2.0.Co;2, 1995.

1182

1183

1184 Table 1. Description of input meteorological variables

Variable (units)	Source data	Ancillary files	Assumptions	Height
Air temperature (K)	MORECS air temperature	IHDTM elevation	Lapsed to IHDTM elevation	1.2 m
Specific humidity (kg kg^{-1})	MORECS vapour pressure, air temperature	IHDTM elevation	Lapsed to IHDTM elevation Constant air pressure	1.2 m
Downward LW radiation (W m^{-2})	MORECS air temperature, vapour pressure, sunshine hours	IHDTM elevation	Constant cloud base height	1.2 m
Downward SW radiation (W m^{-2})	MORECS sunshine hours	IHDTM elevation Spatially-varying aerosol correction	No time-varying aerosol correction	1.2 m
Wind speed (m s^{-1})	MORECS wind speed	ETSU average wind speeds	Wind speed correction is constant	10 m
Precipitation (kg m^{-2} s^{-1})	CEH-GEAR precipitation	-	No transformations performed	n/a
Daily temperature range (K)	CRU TS 3.21 daily temperature range	-	No spatial interpolation from 0.5° resolution. No temporal interpolation (constant values for each month)	1.2 m

Surface air pressure (Pa)	WFD air pressure	IHDTM elevation	Mean-monthly values from WFD used (each year has same values). Lapsed to IHDTM elevation. No temporal interpolation (constant values for each month).	n/a

1185
1186

1187 Table 2: Rate of change of annual means of meteorological and potential evapotranspiration
1188 variables in Great Britain. Bold indicates trends that are significant at the 5% level. The
1189 ranges are given by the 95% CI.

Variable	Rate of change ± 95% CI				
	Great Britain	England	Scotland	Wales	English lowlands
Air temperature (K dec^{-1})	**0.21 ± 0.15**	**0.23 ± 0.14**	**0.17 ± 0.12**	**0.21 ± 0.15**	**0.25 ± 0.17**
Specific humidity (g kg^{-1} dec^{-1})	**0.049 ± 0.037**	**0.054 ± 0.04**	**0.040 ± 0.036**	**0.055 ± 0.037**	**0.053 ± 0.044**
Downward SW radiation (W m^{-2} dec^{-1})	**1.0 ± 0.8**	**1.3 ± 1.0**	0.5 ± 0.6	**1.1 ± 0.9**	**1.5 ± 1.0**
Downward LW radiation (W m^{-2} dec^{-1})	**0.50 ± 0.48**	0.45 ± 0.48	**0.58 ± 0.48**	0.50 ± 0.55	0.42 ± 0.48
Wind speed (m s^{-1} dec^{-1})	**-0.18 ± 0.09**	**-0.16 ± 0.09**	**-0.20 ± 0.10**	**-0.25 ± 0.16**	**-0.13 ± 0.07**
Precipitation (mm d^{-1} dec^{-1})	**0.08 ± 0.06**	0.04 ± 0.06	**0.14 ± 0.09**	0.08 ± 0.09	0.03 ± 0.05
Daily temperature range (K dec^{-1})	-0.06 ± 0.06	-0.03 ± 0.06	**-0.13 ± 0.08**	0.00 ± 0.06	-0.04 ± 0.07
PET (mm d^{-1} dec^{-1})	**0.021 ± 0.021**	**0.025 ± 0.024**	**0.015 ± 0.015**	0.017 ± 0.021	**0.03 ± 0.026**
Radiative component of PET (mm d^{-1} dec^{-1})	**0.016 ± 0.010**	**0.018 ± 0.011**	**0.013 ± 0.008**	**0.020 ± 0.013**	**0.018 ± 0.011**
Aerodynamic component of PET (mm d^{-1} dec^{-1})	0.007 ± 0.011	0.009 ± 0.013	0.004 ± 0.009	0.001 ± 0.013	0.015 ± 0.015
PETI (mm d^{-1} dec^{-1})	0.019 ± 0.020	**0.023 ± 0.023**	0.014 ± 0.014	0.016 ± 0.020	**0.028 ± 0.025**

1190

1191 Table 3. Contributions to the rate of change of PET and its radiative and aerodynamic
1192 components. For each variable, the first column shows the contribution calculated using
1193 regional averages, along with the associated 95% CI. The second column shows the
1194 contribution calculated at 1 km resolution, then averaged over each region. The uncertainty on
1195 this value is difficult to calculate as the pixels are highly spatially correlated, so the
1196 uncertainty range from the regional analysis is used in Fig. 13.

a) Contribution to rate of change of PET (mm d^{-1} $decade^{-1}$)

	Air temperature		Specific humidity		Wind speed		Downward LW		Downward SW		Total	
	Regional	Pixel	Regional	Pixel	Regional	Pixel	Regional	Pixel	Regional	Pixel	Regional	Pixel
England	**0.041 ± 0.025**	0.039	**-0.025 ± 0.019**	-0.024	**-0.010 ± 0.005**	-0.007	0.005 ± 0.006	0.005	**0.013 ± 0.009**	0.012	0.025 ± 0.034	0.024
Scotland	**0.029 ± 0.021**	0.023	**-0.020 ± 0.018**	-0.017	**-0.010 ± 0.005**	-0.007	**0.006 ± 0.005**	0.006	0.005 ± 0.005	0.004	0.010 ± 0.029	0.008
Wales	**0.039 ± 0.028**	0.036	**-0.026 ± 0.018**	-0.025	**-0.011 ± 0.007**	-0.009	0.006 ± 0.006	0.006	**0.010 ± 0.009**	0.009	0.017 ± 0.036	0.017
English lowlands	**0.043 ± 0.029**	0.042	**-0.024 ± 0.020**	-0.023	**-0.008 ± 0.004**	-0.008	0.005 ± 0.006	0.005	**0.015 ± 0.010**	0.015	0.031 ± 0.038	0.030
Great Britain	**0.037 ± 0.026**	0.031	**-0.023 ± 0.018**	-0.022	**-0.010 ± 0.005**	-0.007	**0.006 ± 0.005**	0.005	**0.010 ± 0.007**	0.007	0.019 ± 0.033	0.014

b) Contribution to rate of change of radiative component of (mm d^{-1} $decade^{-1}$)

	Air temperature		Specific humidity		Wind speed		Downward LW		Downward SW		Total	
	Regional	Pixel	Regional	Pixel	Regional	Pixel	Regional	Pixel	Regional	Pixel	Regional	Pixel
England	**-0.009 ± 0.006**	-0.009	n/a	n/a	**0.009 ± 0.005**	0.007	0.005 ± 0.006	0.005	**0.014 ± 0.010**	0.013	**0.018 ± 0.013**	0.016
Scotland	**-0.006 ± 0.005**	-0.006	n/a	n/a	**0.009 ± 0.004**	0.007	**0.006 ± 0.005**	0.006	0.005 ± 0.005	0.004	**0.014 ± 0.010**	0.012
Wales	**-0.007 ± 0.005**	-0.007	n/a	n/a	**0.014 ± 0.009**	0.013	0.006 ± 0.006	0.006	**0.010 ± 0.009**	0.010	**0.023 ± 0.015**	0.022
English lowlands	**-0.010 ± 0.007**	-0.010	n/a	n/a	**0.007 ± 0.004**	0.006	0.005 ± 0.006	0.005	**0.016 ± 0.011**	0.015	**0.017 ± 0.014**	0.017
Great Britain	**-0.008 ± 0.006**	-0.007	n/a	n/a	**0.009 ± 0.005**	0.007	**0.006 ± 0.006**	0.006	**0.010 ± 0.008**	0.008	**0.017 ± 0.012**	0.013

c) Contribution to rate of change of aerodynamic component of PET (mm d^{-1} $decade^{-1}$)

	Air temperature		Specific humidity		Wind speed		Downward LW		Downward SW		Total	
	Regional	Pixel	Regional	Pixel	Regional	Pixel	Regional	Pixel	Regional	Pixel	Regional	Pixel

Engla nd	**0.052 ± 0.032**	0.050	**-0.026 ± 0.020**	-0.026	**-0.018 ± 0.010**	-0.015	n/a	n/a	n/a	n/a	**0.007 ± 0.039**	0.009
Scotla nd	**0.037 ± 0.027**	0.033	**-0.021 ± 0.019**	-0.019	**-0.019 ± 0.010**	-0.015	n/a	n/a	n/a	n/a	-0.003 ± 0.034	-0.001
Wales	**0.048 ± 0.035**	0.046	**-0.028 ± 0.019**	-0.027	**-0.026 ± 0.016**	-0.023	n/a	n/a	n/a	n/a	-0.005 ± 0.042	-0.003
Engli sh lowla nds	**0.056 ± 0.037**	0.055	**-0.026 ± 0.021**	-0.025	**-0.015 ± 0.008**	-0.014	n/a	n/a	n/a	n/a	0.015 ± 0.044	0.015
Great Britai n	**0.046 ± 0.033**	0.041	**-0.025 ± 0.019**	-0.023	**-0.020 ± 0.010**	-0.015	n/a	n/a	n/a	n/a	0.002 ± 0.039	0.003

1197
1198

1199 Table 4. Contribution of the trend in each variable to the trends in annual mean PET and its

1200 radiative and aerodynamic components as a percentage of the fitted trend in PET and its

1201 components.

a) Potential evapotranspiration (PET)						
	Air temperature	Specific humidity	Wind speed	Downward LW	Downward SW	Total
England	154 %	-88 %	-22 %	17 %	47 %	108 %
Scotland	150 %	-74 %	-23 %	26 %	18 %	97 %
Wales	200 %	-130 %	-38 %	28 %	50 %	109 %
English lowlands	142 %	-77 %	-20 %	15 %	45 %	105 %
Great Britain	155 %	-87 %	-23 %	19 %	31 %	96 %
b) Radiative component of PET						
	Air temperature	Specific humidity	Wind speed	Downward LW	Downward SW	Total
England	-47 %	n/a	40 %	28 %	71 %	92 %
Scotland	-42 %	n/a	62 %	46 %	36 %	102 %
Wales	-34 %	n/a	69 %	29 %	52 %	116 %
English lowlands	-53 %	n/a	35 %	27 %	86 %	95 %
Great Britain	-44 %	n/a	46 %	31 %	53 %	87 %
c) Aerodynamic component of PET						
	Air temperature	Specific humidity	Wind speed	Downward LW	Downward SW	Total
England	245 %	-115 %	-48 %	n/a	n/a	82 %
Scotland	68 %	-14 %	-33 %	n/a	n/a	21 %
Wales	-135 %	72 %	-42 %	n/a	n/a	-105 %
English lowlands	282 %	-126 %	-47 %	n/a	n/a	109 %
Great Britain	168 %	-76 %	-44 %	n/a	n/a	48 %

1202
1203

1204 Table A1. Details of sites used for validation of meteorological data.

Site (ID)	Latitude	Longitude	Years	Land cover	Citation
Alice Holt (UK-Ham)	51.15	-0.86	2004-2012	Deciduous broadleaf woodland	(Wilkinson et al., 2012; Heinemeyer et al., 2012)
Griffin Forest (UK-Gri)	56.61	-3.80	1997-2001, 2004-2008	Evergreen needleleaf woodland	(Clement, 2003)
Auchencorth Moss (UK-AMo)	55.79	-3.24	2002-2006	Grass and crop	(Billett et al., 2004)
Easter Bush (UK-EBu)	55.87	-3.21	2004-2008	Grass	(Gilmanov et al., 2007; Soussana et al., 2007)

1205

1206 Table A2. Correlation statistics for meteorological variables with data from four sites.

a) Air temperature

Site	r^2	Mean bias	RMSE
Alice Holt	0.95	0.10 K	1.17 K
Griffin Forest	0.94	0.21 K	1.17 K
Auchencorth Moss	0.98	-0.02 K	0.78 K
Easter Bush	0.97	-0.46 K	0.96 K

b) Downward SW radiation

Site	r^2	Mean bias	RMSE
Alice Holt	0.94	-3.01 W m^{-2}	22.92 W m^{-2}
Griffin Forest	0.85	-4.90 W m^{-2}	31.29 W m^{-2}
Auchencorth Moss	0.91	14.27 W m^{-2}	27.96 W m^{-2}
Easter Bush	0.88	5.73 W m^{-2}	27.15 W m^{-2}

c) Mixing ratio

Site	r^2	Mean bias	RMSE
Alice Holt	0.90	-0.02 mmol mol^{-1}	1.09 mmol mol^{-1}
Griffin Forest	0.76	0.08 mmol mol^{-1}	1.56 mmol mol^{-1}

d) Wind speed

Site	r^2	mean bias	RMSE
Alice Holt	0.88	1.24 m s^{-1}	1.45 m s^{-1}
Griffin Forest	0.59	1.36 m s^{-1}	1.81 m s^{-1}
Auchencorth Moss	0.63	-0.38 m s^{-1}	1.37 m s^{-1}
Easter Bush	0.82	0.44 m s^{-1}	1.03 m s^{-1}

e) Surface air pressure

Site	r^2	Mean bias	RMSE
Griffin Forest	0.05	-0.42 hPa	1.38 hPa
Auchencorth Moss	0.01	-1.06 hPa	1.57 hPa
Easter Bush	0.03	0.01 hPa	1.33 hPa

1207
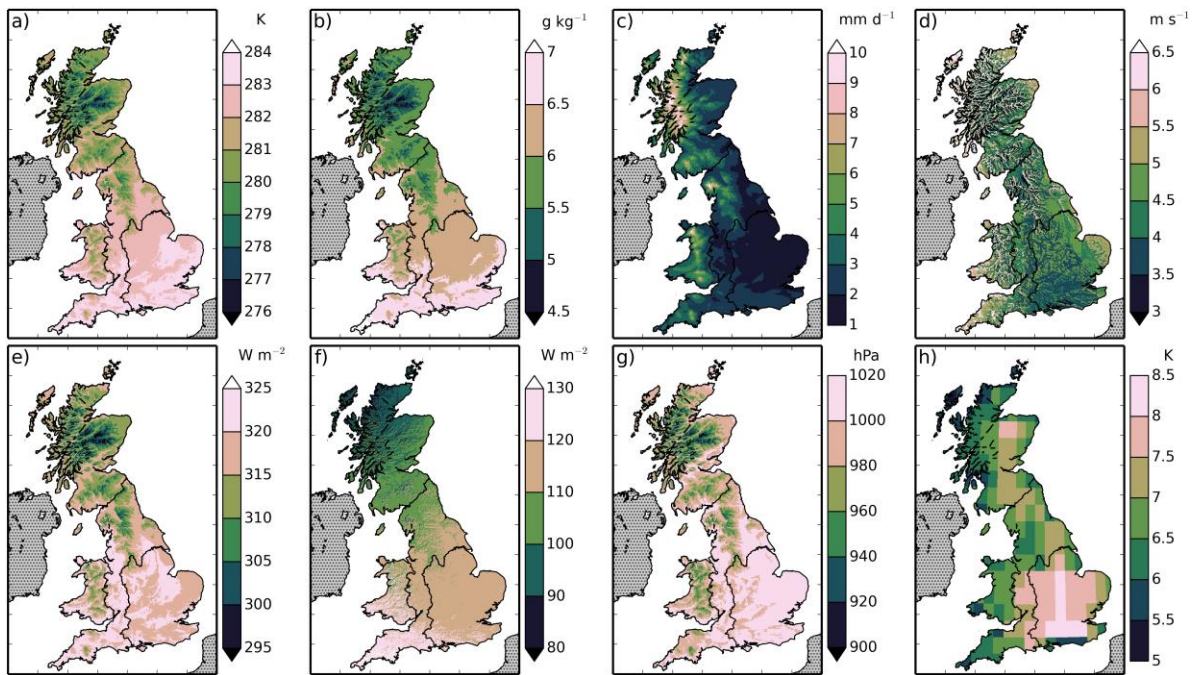
1208

1209 Figure 1. Means of the meteorological variables over the years 1961-2012. The variables are

1210 a) 1.2 m air temperature, b) 1.2 m specific humidity, c) precipitation, d) 10 m wind speed, e)

1211 downward LW radiation, f) downward SW radiation, g) surface air pressure, h) daily air

1212 temperature range.

1213

1214 Figure 2. The regions used to calculate the area means. The English lowlands are a sub-region

1215 of England. England, Scotland and Wales together form the fifth region, Great Britain.
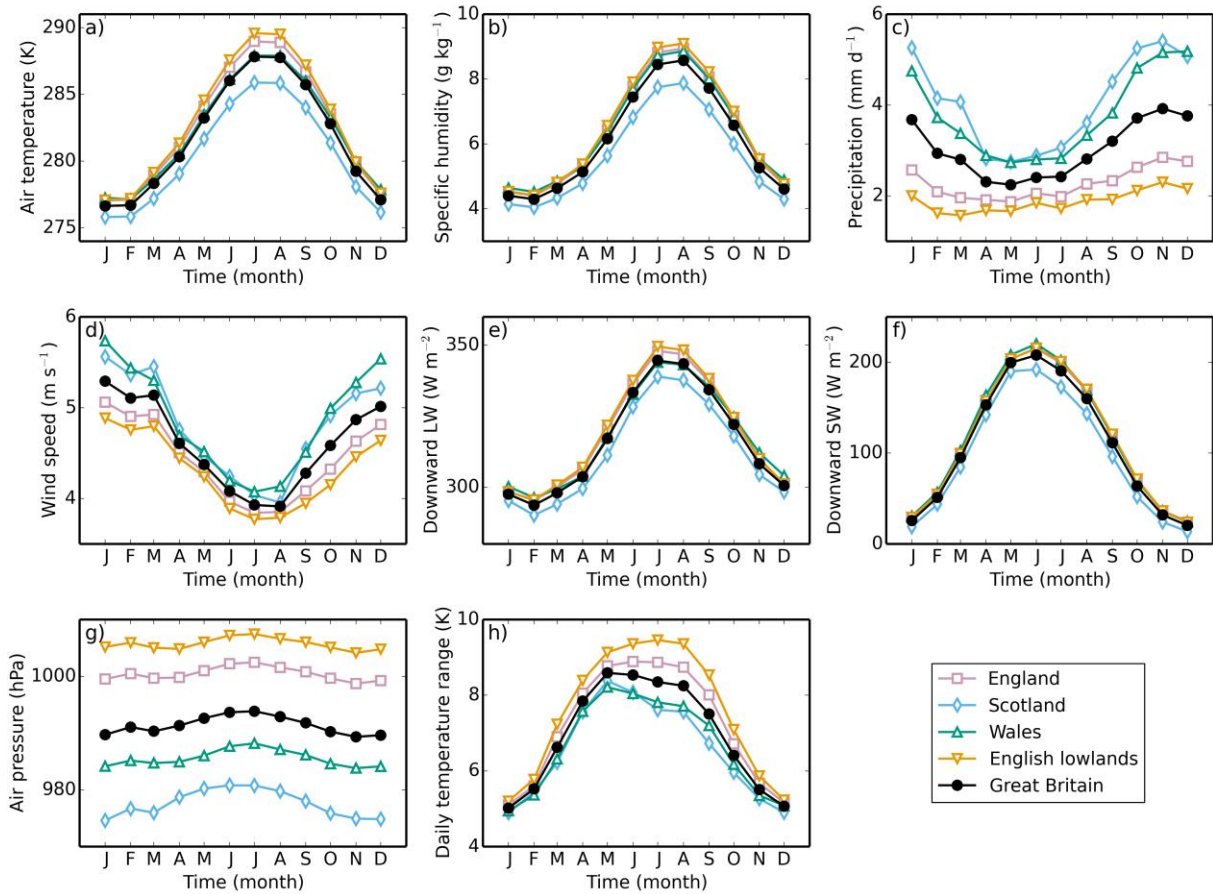
1216

1217   Figure 3. Mean monthly climatology of meteorological variables, a) 1.2 m air temperature, b)

1218   1.2 m specific humidity, c) precipitation, d) 10 m wind speed, e) downward LW radiation, f)

1219   downward SW radiation, g) surface air pressure, h) daily air temperature range, for five

1220   different regions of Great Britain, calculated over the years 1961-2012.

1221
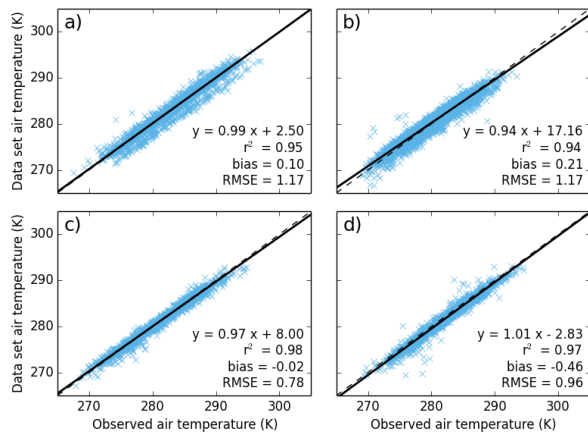
1222

1223 Figure 4. Plot of data set air temperature against daily mean air temperature at four sites. The

1224 dashed line shows the one to one line, while the solid line shows the linear regression, the

1225 equation of which is shown in the lower right of each plot, along with the r^2 value, the mean

1226 bias and the RMSE. The sites are a) Alice Holt; b) Griffin Forest; c) Auchencorth Moss; d)

1227 Easter Bush.

1228
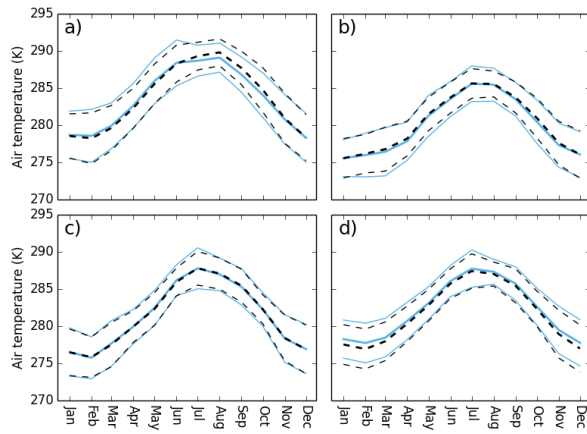
 Figure 5. Mean monthly climatology of the dataset (blue, solid lines) and observed air
 temperatures (black, dashed lines), calculated for the period of observations. The thicker lines
 show the means, while the thinner lines show the standard errors on each measurement. Sites
 as in Fig. 4.
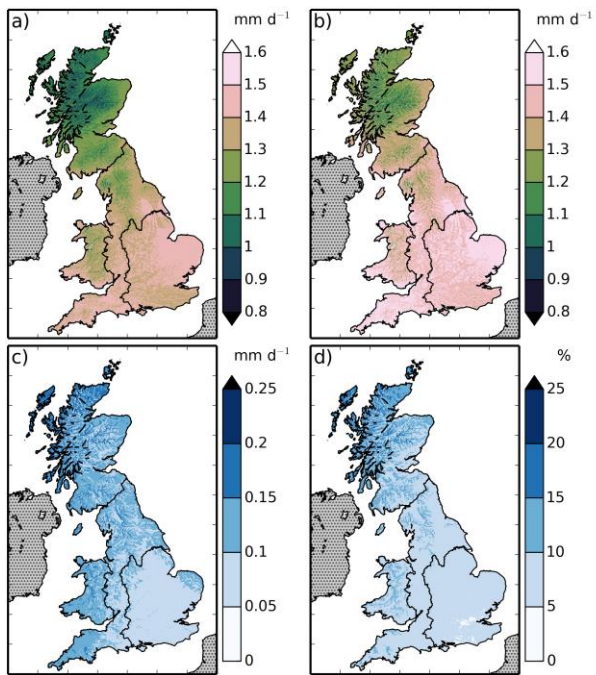
1236

1237 Figure 6. Mean a) PET, b) PETI, c) absolute difference between PETI and PET and d) relative

1238 difference calculated over the years 1961-2012.
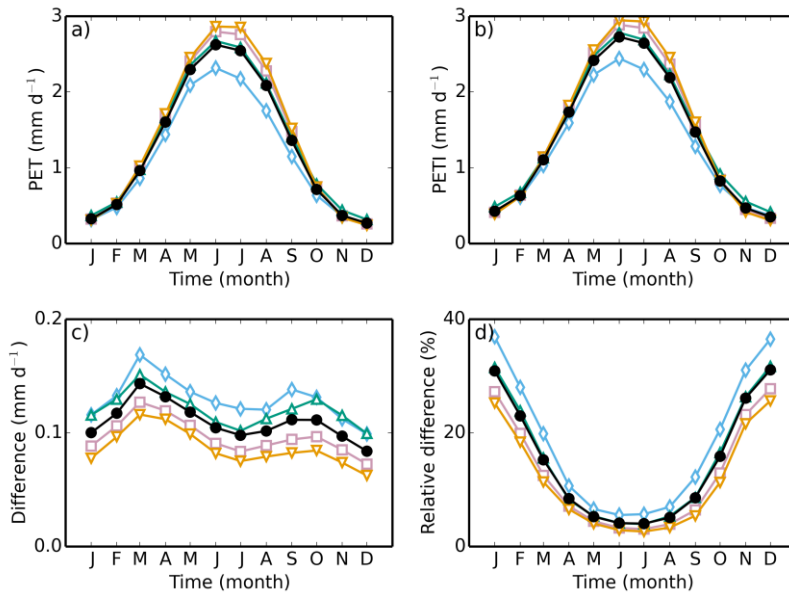
1239

1240   Figure 7. Mean monthly climatology of a) PET, b) PETI, c) absolute difference between PETI

1241   and PET, d) relative difference, for five different regions of Great Britain, calculated over the

1242   years 1961-2012. Symbols as in Fig. 3.
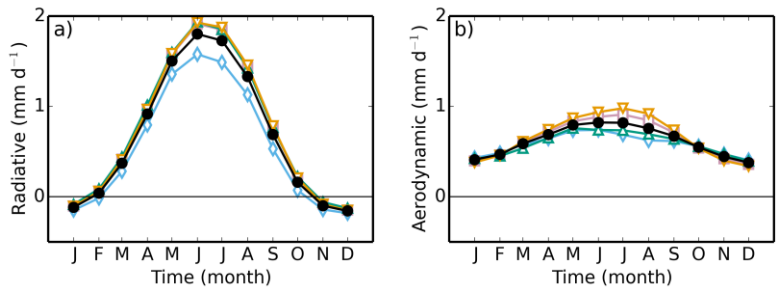
1243

1244 Figure 8. Mean-monthly climatology of the a) radiative and b) aerodynamic components of the

1245 PET for five different regions of Great Britain, calculated over the years 1961-2012. Symbols

1246 as in Fig. 3.
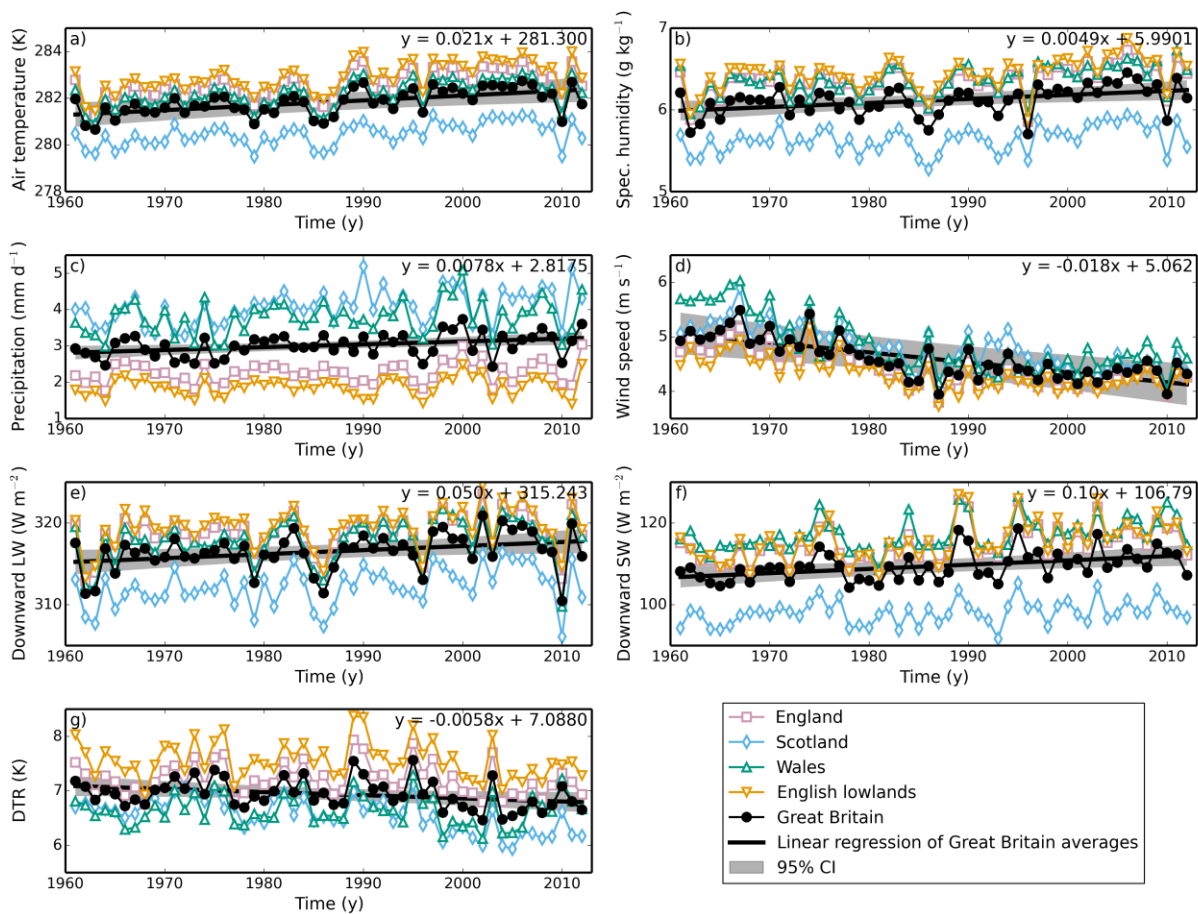
1247

1248 Figure 9. Annual means of the meteorological variables, a) 1.2 m air temperature, b) 1.2 m

1249 specific humidity, c) precipitation, d) 10 m wind speed, e) downward LW radiation, f)

1250 downward SW radiation, g) daily air temperature range, over five regions of Great Britain. The

1251 solid black lines show the linear regression fit to the Great Britain annual means, while the grey

1252 strip shows the 95% CI of the same fit, assuming a non-zero lag-1 correlation coefficient. The

1253 equation of this fit is shown in the top right-hand corner of each plot.
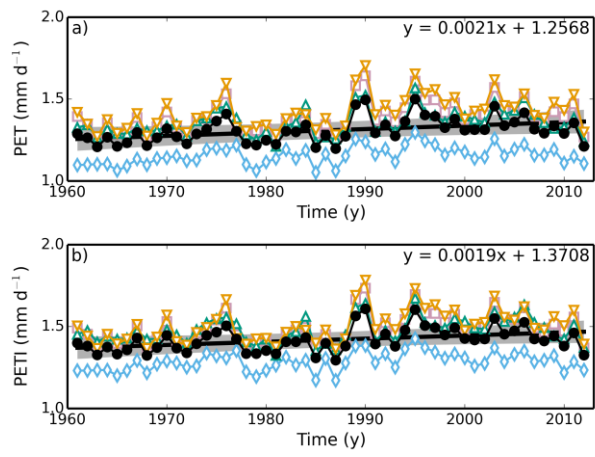
1254

Figure 10. Annual means of a) PET and b) PETI for five regions of Great Britain. Symbols as in Fig. 9.

1255

1256

1257
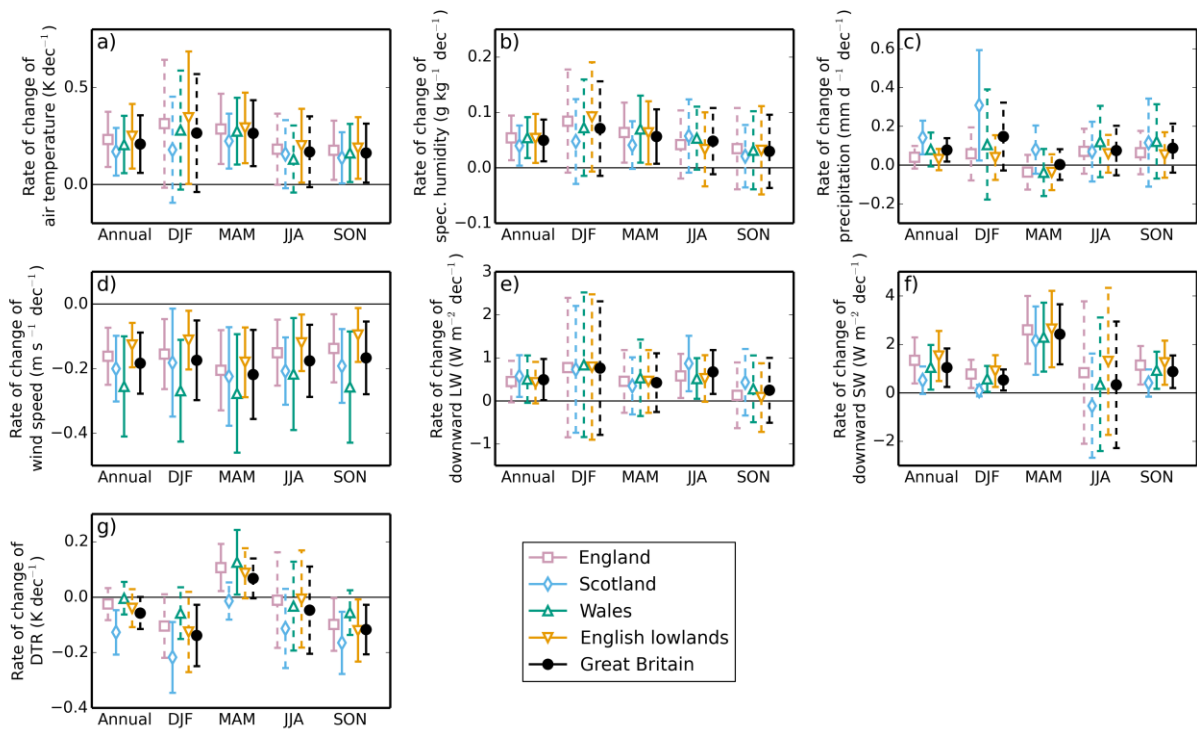
1258

1259   Figure 11. Rate of change of annual and seasonal means of meteorological variables, a) 1.2 m

1260   air temperature, b) 1.2 m specific humidity, c) precipitation, d) 10 m wind speed, e) downward

1261   LW radiation, f) downward SW radiation, g) daily air temperature range, for five regions of

1262   Great Britain for the years 1961-2012. Error bars are the 95% CI calculated assuming a non-

1263   zero lag-1 correlation coefficient. Solid error bars indicate slopes that are statistically significant

1264   at the 5% level, dashed error bars indicate slopes that are not significant at the 5% level.

1265
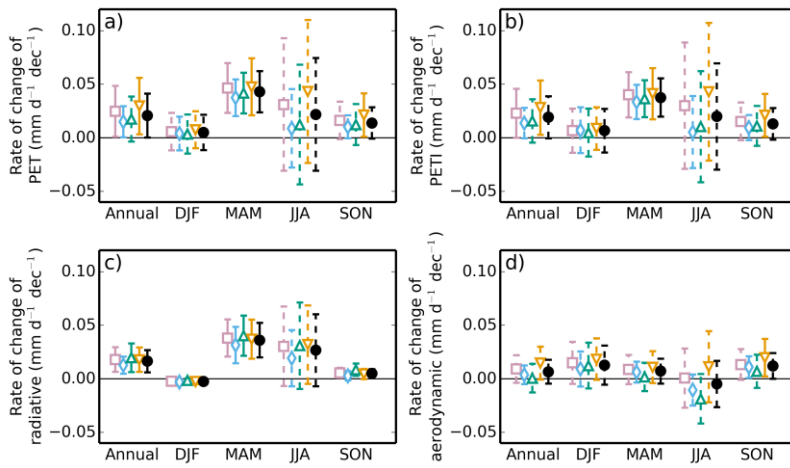
1266

1267 Figure 12. Rate of change of annual and seasonal means of a) PET, b) PETI, c) the radiative

1268 component of PET and d) the aerodynamic component of PET for five regions of Great Britain

1269 for the years 1961-2012. Symbols as in Fig. 11.
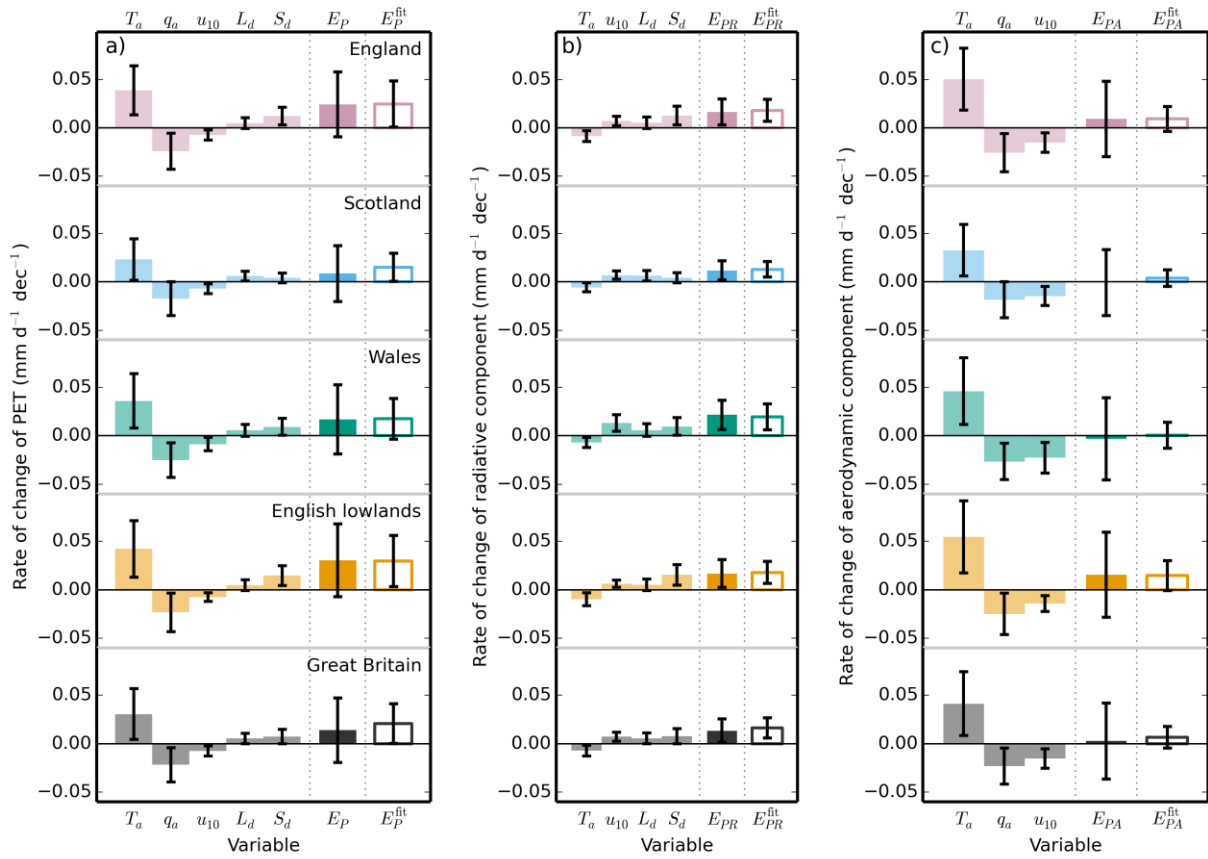
1270

Figure 13. The contribution of the rate of change of each meteorological variable to the rate of change of a) PET, b) the radiative component and c) the aerodynamic component. The first five (four; three) bars are the contribution to the rate of change of annual mean PET from the rate of change of each of the variables, calculated per pixel, than averaged over each region. Each bar has an error bar showing the 95% CI on each value. Since the pixels are highly spatially correlated, we use the more conservative CI calculated by applying this analysis to the regional means. The next bar is the sum of the other bars and shows the attributed rate of change of annual mean PET. The final bar shows the slope and its associated CI obtained from the linear regression of the mean annual PET for each region.

1280
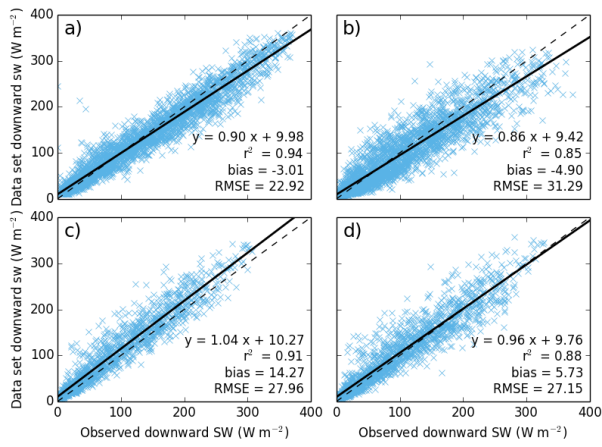
1281

1282   Figure A1. Plot of data set downward SW radiation against daily mean downward SW radiation

1283   at four flux sites. Symbols and sites as in Fig. 4.

1284
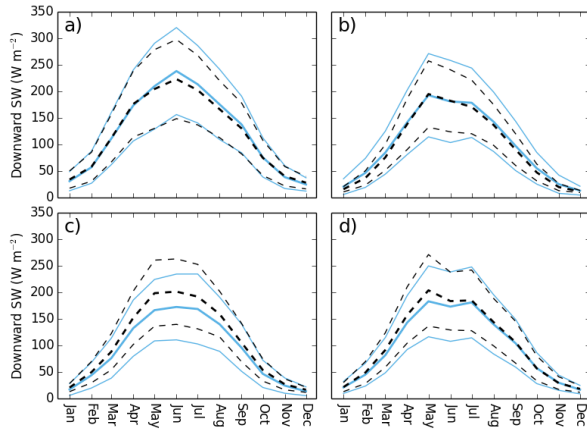
1287 Figure A2. Mean monthly climatology of the dataset (blue, solid lines) and observed air

1288 temperatures (black, dashed lines), calculated for the period of observations. Symbols as in Fig.

1289 5, sites as in Fig. 4.

1290
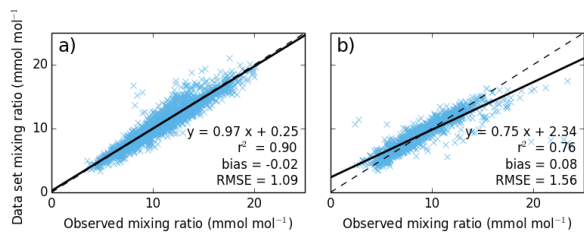
1291

1292   Figure A3. Plot of mixing ration calculated using dataset meteorology against daily mean

1293   observed mixing ratio at four sites. Symbols as in Fig. 4. The sites are a) Alice Holt and b)

1294   Griffin Forest.

1295
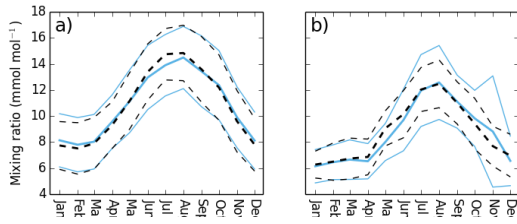
1298   Figure A4. Mean monthly climatology of the dataset (blue, solid lines) and observed mixing

1299   ratio (black, dashed lines), calculated for the period of observations. Symbols as in Fig. 5. Sites

1300   as in Fig. A3.

1301
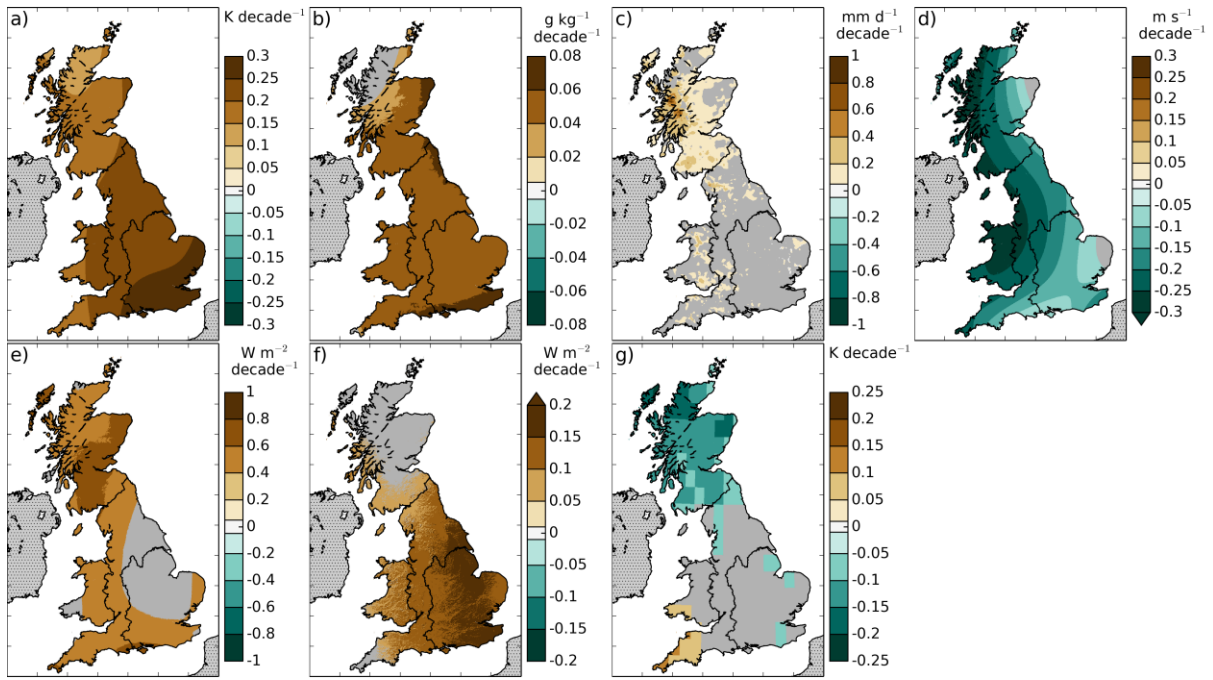
1302

1303 Figure B1. Rate of change of the meteorological variables, a) 1.2 m air temperature, b) 1.2 m
1304 specific humidity, c) precipitation, d) 10 m wind speed, e) downward LW radiation, f)
1305 downward SW radiation, g) surface air pressure, h) daily air temperature range over the period
1306 1961-2012. Areas for which the trend was not significant are shown in grey.

1307
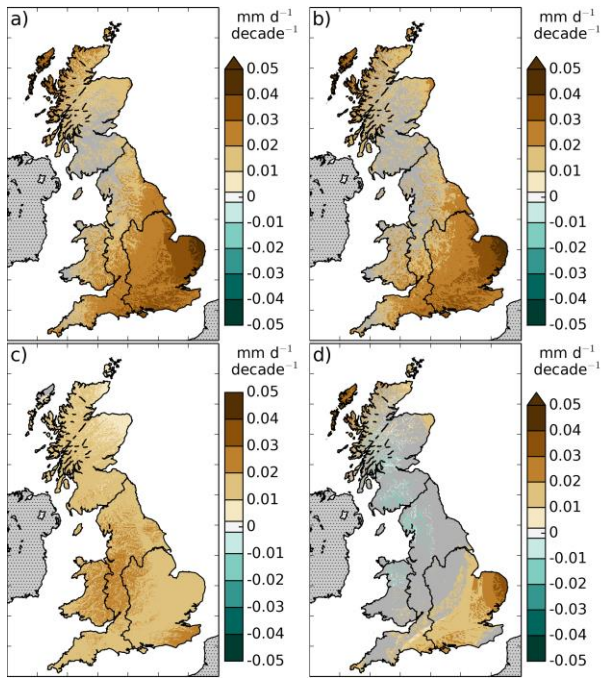
1308

1309   Figure B2. Rate of change of a) PET, b) PETI, c) the radiative component of PET, d) the
1310   aerodynamic component of PET over the period 1961-2012. Areas for which the trend was
1311   not significant are shown in grey.